THE LOWER TRIASSIC BJORNE FORMATION:

FROM DEPOSITION TO DIAGENESIS IN THE EASTERN SVERDRUP

BASIN, ELLESMERE ISLAND, NUNAVUT, CANADA

Derrick W. Midwinter

Submitted in Partial Fulfillment of the Requirements
for the Degree of Bachelor of Science, Honours
Department of Earth Sciences
Dalhousie University, Halifax, Nova Scotia
March 2012

Distribution License

DalSpace requires agreement to this non-exclusive distribution license before your item can appear on DalSpace.

NON-EXCLUSIVE DISTRIBUTION LICENSE

You (the author(s) or copyright owner) grant to Dalhousie University the non-exclusive right to reproduce and distribute your submission worldwide in any medium.

You agree that Dalhousie University may, without changing the content, reformat the submission for the purpose of preservation.

You also agree that Dalhousie University may keep more than one copy of this submission for purposes of security, back-up and preservation.

You agree that the submission is your original work, and that you have the right to grant the rights contained in this license. You also agree that your submission does not, to the best of your knowledge, infringe upon anyone's copyright.

If the submission contains material for which you do not hold copyright, you agree that you have obtained the unrestricted permission of the copyright owner to grant Dalhousie University the rights required by this license, and that such third-party owned material is clearly identified and acknowledged within the text or content of the submission.

If the submission is based upon work that has been sponsored or supported by an agency or organization other than Dalhousie University, you assert that you have fulfilled any right of review or other obligations required by such contract or agreement.

Dalhousie University will clearly identify your name(s) as the author(s) or owner(s) of the submission, and will not make any alteration to the content of the files that you have submitted.

If you have questions regarding this license please contact the repository manager at dalspace@dal.ca.

Grant the distribution license by signing and dating below.

_____   _____

Name of signatory   Date

Department of Earth Sciences
Halifax, Nova Scotia
Canada B3H 4J1
(902) 494-2358
FAX (902) 494-6889

DATE: <u>MARCH 17, 2012</u>

AUTHOR: <u>DERRICK W. MIDWINTER</u>

TITLE: <u>THE LOWER TRIASSIC BJORNE FORMATION: FROM DEPOSITION TO</u>

   <u>DIAGENESIS IN THE EASTERN SVERDRUP BASIN, ELLESMERE</u>

   <u>ISLAND, NUNAVUT, CANADA</u>

Degree: <u>B.Sc.</u>   Convocation: <u>May</u>   Year: <u>2012</u>

   Permission is herewith granted to Dalhousie University to circulate and to have copied for non-commercial purposes, at its discretion, the above title upon the request of individuals or institutions.

_____
Signature of Author

ABSTRACT

The Bjorne Formation is a predominantly sandstone unit in the Sverdrup Basin in the northern part of the Canadian Arctic Islands. The Lower Triassic succession of the Bjorne Formation and coeval Blind Fiord Formation nears 2,000 m thickness in two depocentres in the basin, and 1,000 m along the margins, a significant portion of the 13,000 m of Carboniferous to Tertiary basin fill. The Early Triassic represents a period of active subsidence and major infilling of the Sverdrup Basin. The study location is on Fosheim Peninsula, Ellesmere Island with the outcrop representing the eastern margin of the basin during three pulses of Early Triassic sedimentation. The sandstone members, Cape Butler, Pell Point and Cape O'Brien, are separated by thin marine shale units, which represent basin-wide transgression.

Each member comprises several hundred metres of stacked sandstones with some members having red siltstone interbeds. While each member comprises of successions composed primarily of upper flow regime, to the transition to lower flow regime beds, the lithofacies proportions are not identical. The Cape Butler Member is composed principally of upper flow regime bedforms with scarce dune stratification, whereas the Pell Point and Cape O'Brien members are predominantly cross-stratified with parallel stratification. Siltstone beds have climbing ripples, shrinkage cracks, and bioturbation. The architecture of the sandstone units represents sand sheets as they appear laterally extensive and multistory with little suggestion of major channel forms. The presence of trace fossils provides evidence of sub-aqueous conditions, although the degree of marine influence is not clear. The thick fluvial sandstones and marine shale tongues suggest the braided fluvial system passed directly basinward into a marine-influenced environment. These associations of sedimentary features suggest episodic and rapid sedimentation within the spectrum of a braid-delta.

Deposition took place immediately following the Permo/Triassic boundary. Extinction of many vegetational taxa at that boundary could have influenced fluvial styles because vegetation helps stabilize banks. The extinction event and the proximity to the Siberian Traps affected the depositional regime and sediment flux across the boundary.

Petrographic analysis of the sandstone identifies it as a quartzarenite to sublitharenite with early pore-filling calcite cement and late grain-replacive, pore-filling dolomite-ankerite rhombohedra. The calcite cement occludes primary porosity, and the rhombohedra occlude secondary porosity created by grain dissolution. Analysis of the provenance is indicative of a craton interior and recycled orogen source. Based on thermal maturation within the oil window, thickness of the sandstones, high permeability of some core samples, shale seals, and possible organic-rich source rocks, the Bjorne Formation is a prospective hydrocarbon reservoir.

Keywords: Bjorne Formation, Sverdrup Basin, Early Triassic, Sandstone, Braid-Delta, Ephemeral, Late Permian Extinction, Upper Flow Regime, Carbonate Cementation

TABLE OF CONTENTS

TABLE OF FIGURES

TABLE OF TABLES

ACKNOWLEDGEMENTS

CHAPTER 1: INTRODUCTION

1.1 The Bjorne Formation

The Bjorne Formation is an extensive and continuous formation exceeding 1,000 m in thickness along the south and east margins of the Sverdrup Basin in the Canadian Arctic Archipelago (Fig. 1.1). Earliest Mesozoic strata represent a new depositional regime in the Sverdrup Basin following the end Permian extinction. The climate was warm and dry, sedimentation was dominated by siliciclastics, and marine life was nominal (Embry and Beauchamp, 2008). During the beginning of the Mesozoic, the Canadian Arctic Archipelago was positioned at 40°N (Irving and Irving, 1982). With an influx of sediment, major deltas began prograding into the basin along the margins of the Sverdrup Basin, represented by the Bjorne Formation, an Lower Triassic sandstone unit. The Bjorne Formation began infilling the basin predominantly from the east and south margins. It is stratigraphically equivalent to the distal shale/siltstone unit called the Blind Fiord Formation. The Bjorne and Blind Fiord formations represent a major siliciclastic infilling of the Sverdrup Basin.

The Bjorne Formation has three formally named sandstone members, the Cape Butler, Pell Point and Cape O'Brien (Embry, 1986). Formation thickness exceeds 2,000 m in the depocentres (Fosheim Peninsula, Ellesmere Island and Sabine Peninsula, Melville Island) and will be referred to as the Fosheim and Melville segments. The Bjorne Formation consists mainly of fine- to medium grained sandstone with minor red siltstone interbeds deposited in a predominantly fluvial to marine environment (Embry, 1991). Along the eastern margin, two tongues of shale known as the Smith Creek and Svartfjeld members penetrate the Bjorne Formation, representing basin wide transgression. These two members are part of the distal Blind Fiord Formation, but can be included in the Bjorne Formation in the proximal setting.
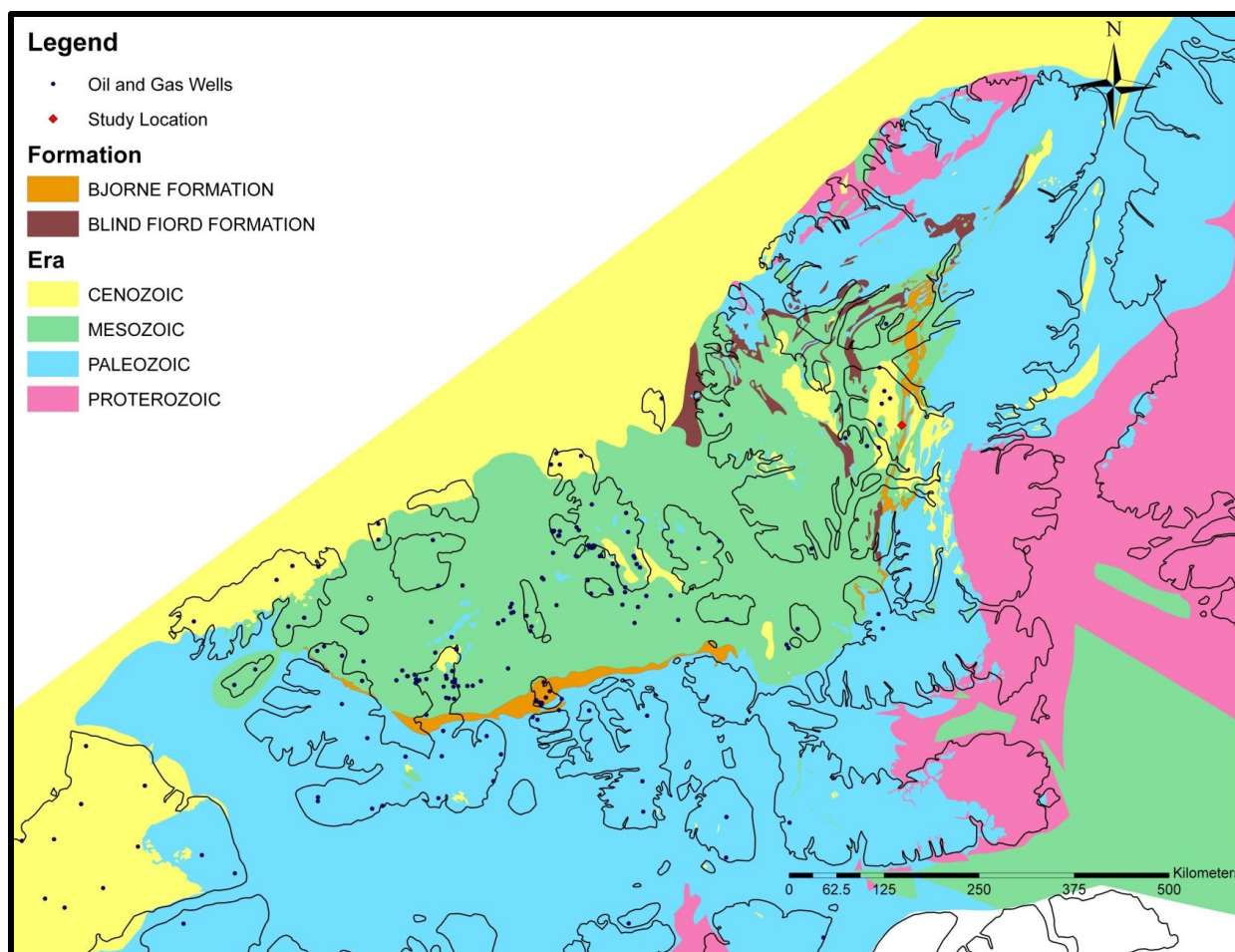
Figure 1.1: Regional geology of the Canadian Arctic Archipelago (modified after Okulitch, 1991 and digitized by staff at GSC Calgary).

The relative age of the Bjorne Formation was determined using biostratigraphy from correlative intervals of Blind Fiord that yielded the ammonoid assemblages upon which Tozer (1965) based his Triassic Griesbachian, Dienerian, Smithian and Spathian stages.

The age of some detrital grains was discovered using zircons from the sandstone. Miller et al. (2006) sampled a Smithian, braided stream facies of the Bjorne Formation. Zircon grains from Lower Triassic sandstones in the Arctic predominantly date in the Ordovician and Mesoproterozoic (~1.2 Ga), but otherwise the sample from the Bjorne Formation is very different, in that it has an absence of Cambrian, late Precambrian and Paleoproterozoic or
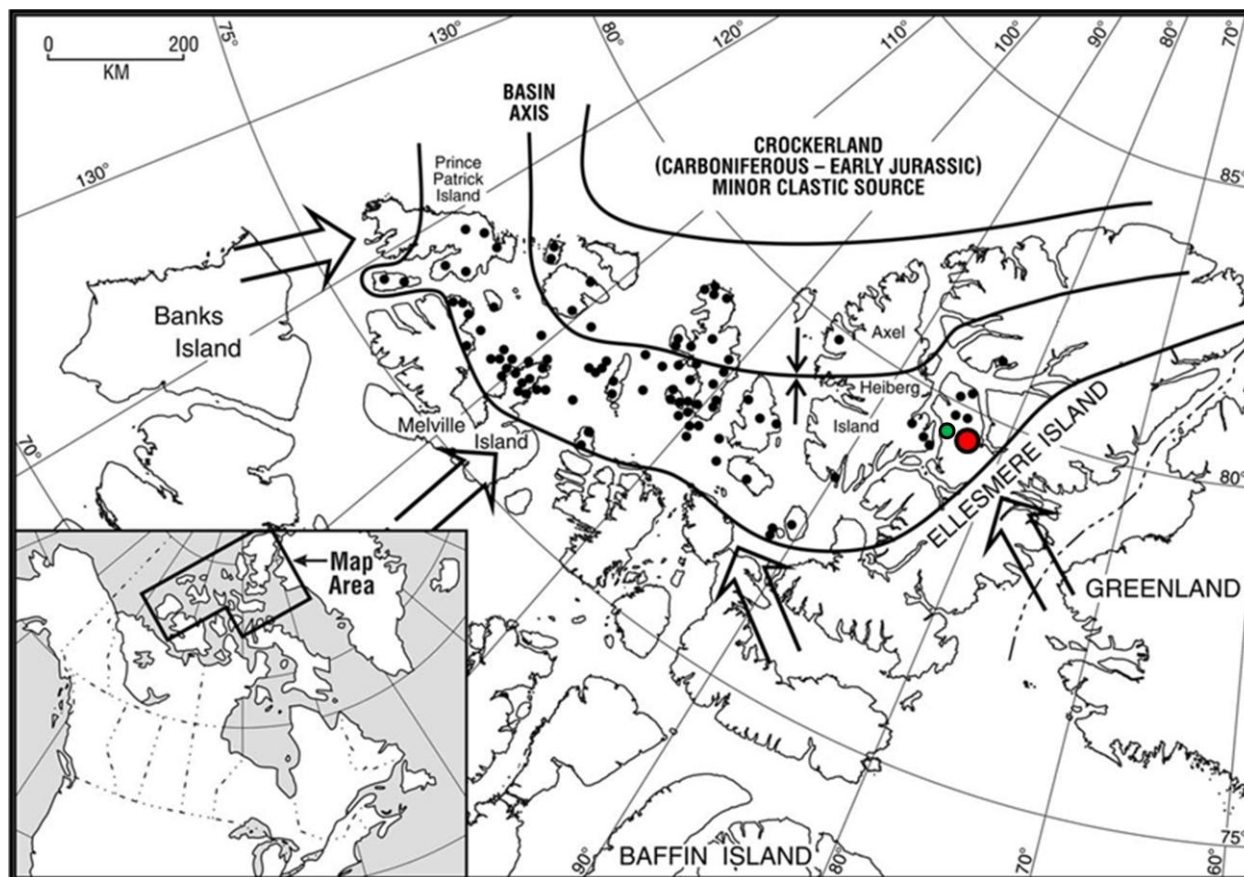
Figure 1.2: Map of the Arctic and Sverdrup Basin with basin axis. Black dots represent 120 wells drilled in basin. The main source areas from the south and east are indicated by arrows. Study area highlighted by red circle, green circle represents closest well, Fosheim N-27 (modified after Embry and Beauchamp, 2008).

Archean zircons. Given the inferred southeast source for the Bjorne Formation (representing flow across the Canadian and Greenland Precambrian Shields), the older ages can be explained (Miller et al., 2006). Deposition occurred during three transgression-regression cycles and the sediment was derived largely from Devonian siliciclastics that flanked the margin and extended over the craton (Embry and Beauchamp, 2008).

From a global perspective, the plate-tectonic setting for the Early Triassic features a widespread assembly of the earth's continental blocks into the Pangaean supercontinent (Harrison, 2005).

1.2 Regional Geology

The Bjorne Formation was deposited along the margins of the Sverdrup Basin (Fig. 1.2), which is a major depocentre in the Arctic Islands with up to 13,000 m of Carboniferous to Paleogene marine and non-marine sedimentary rocks, basaltic flows and gabbroic intrusions (Balkwill, 1978). The northern margin of the North American craton lies near the southern edge of the basin. During the Carboniferous, the Sverdrup Basin began as a rift basin on top of lower Paleozoic strata. The upper Paleozoic strata are up to 5,000 m thick and represent a shelf to deep basin setting. In the Mesozoic, there was abundant sedimentation that generally exceeded basin subsidence which allowed up to 9,000 m of sediment to be deposited in the centre of the basin, with the Sverdrup Basin containing the most complete Mesozoic section in the Arctic (Embry, 1991).

In the Early Triassic, the two main depocentres of Bjorne and Blind Fiord strata, the Fosheim and Melville segments, have thicknesses exceeding 2,000 m, whereas the strata is commonly less than 1,200 m along the margins. The bulk of the sediment supply was from the south and east of the Sverdrup Basin, with sediment derived principally from the Devonian Clastic Wedge rather than the Precambrian Shield because from Ordovician through Cretaceous time, the Shield was covered by sedimentary rock (Patchett et al., 2004). Northerly-derived sediment into the Sverdrup Basin was unlikely to have influenced the Bjorne Formation in the study area as it was a nominal sediment source for the south and east margins. Embry (1993) proposed that, from Carboniferous to mid-Jurassic, there was a large landmass, named Crockerland (Fig. 1.2), located to the north of the basin, which was based on regional stratigraphic studies of the Mesozoic succession and interpretations of the plate tectonic relationships between northern Alaska, the Canadian Arctic Islands and Svalbard.

Widespread Cretaceous diabase sills and dykes intruded the northeastern region are related to the opening of the adjacent Canada Basin and to the Alpha Ridge plume, a hot spot track in the Amerasian Basin (Embry and Beauchamp, 2008). Carboniferous evaporite began diapirism in the basin beginning in the early Mesozoic due to sediment loading inducing evaporite mobilization and continued episodically to the Paleogene from related to folding and faulting. The Eurekan Orogeny took place during the Early Paleogene driven by the counter-clockwise rotation of Greenland which created uplift and deformation primarily along the eastern margin (Embry and Beauchamp, 2008).

Numerous oil and gas fields have been discovered near anticlinal swells formed during the Eurekan Orogeny and salt diapir emplacement. These and other structures provide effective traps, which along with widespread source rocks and porous sandstone reservoirs, indicates that there is an effective hydrocarbon system in the basin. The Sverdrup Basin is an established petroliferous, rift/sag basin with 17 discovered oil and gas fields. The Lower Triassic pinch-outs of these porous sands in suitable structural orientations provide good petroleum prospects because they were present during maturation and migration of the Triassic-sourced hydrocarbons (Embry, 2011). The Bjorne Formation contains hydrocarbons in part as oil sands on Melville Island and oil shows in the top member of the Bjorne Formation in a well (Fosheim N-27) drilled at Fosheim Peninsula on Ellesmere Island.

1.3 Previous Work

The type section of the Bjorne Formation is in southwestern Ellesmere Island and was defined by Tozer (1963), who subsequently described the Bjorne Formation along the basin margins. Roy (1972) also described the Bjorne Formation on southern and central Ellesmere Island. These descriptions allowed Embry (1986) to compile the boundaries, lithology, thickness and

Unit	Lithology	Thickness	Distribution	Relation to Other Units	Age
Bjorne Fm[1]	fg-mg sandstone, often weathers red or brown; conglomerate are common. Thin red shales occur throughout	Ranges from 60 to 1440m	Occurs parallel to southerly and westerly-trending margin of the Sverdrup Basin between northern Ellesmere Island and Prince Patrick Island	Conformably overlain by the Schei Point Gp in most areas and unconformably overlies Permian strata. Bjorne beds are contemporaneous with and form the equivalents of the basinal Blind Fiord Fm	Lower Triassic
Cape Butler Mbr[2]	fg-mg sandstone with interbeds of red, green or grey shale and siltstone	Ranges from few metres near its shale-out edge to 375m	Occurs along the southern and eastern margins except in the Melville Island area where the Bjorne Fm is undivided	The member conformably overlies the Confederation Point Member of the Blind Fiord Fm, and overlain by the Smith Creek Mbr	Griesbachian to Dienerian
Pell Point Mbr[2]	fg-mg sandstone with interbeds of red, green or grey shale and siltstone	Thickest near edge of basin and reaches 555m, and eventually disappears basinward	Occurs along the southern and eastern margins except in the Melville Island area where the Bjorne Fm is undivided	Conformably overlies the Smith Creek Mbr, and conformably overlain by the Svartfjeld Mbr	Smithian
Cape O'Brien Mbr[2]	fg-mg sandstone with interbeds of red, green or grey shale and siltstone	Thickest in Fosheim Peninsula area and approaches 500m, thins basinward	Occurs along the southern and eastern margins except in the Melville Island area where the Bjorne Fm is undivided	Conformably overlies the Svartfjeld Mbr and overlain by the Murray Harbour Fm, which varies from conformable to unconformable	Spathian
Blind Fiord Fm[1]	Mainly grey to green, partly micaceous siltstone, interbedded with grey shale in some areas	At type locality, about 1120m thick, but varies from 330m to 1210	Outcrops in north-east trending belt from Axel Heiberg Island to northwestern Ellesmere Island; probably present throughout the basinal centre	Basinal equivalent of the Bjorne Fm, Blind siltstones are paraconformably underlain by the Permian cherty limestones at their type locality and is overlain by the Blaa Mountain Fm	Lower Triassic
Confederation Point Member[2]	Medium to dark grey, silty shale with interbeds of argillaceous siltstone that become more common upwards	525m thick at type locality, and thins to 100m along the margin	Occurs in northern Ellesmere and Axel Heiberg islands, recognized in wells in the western Sverdrup Basin	Abruptly overlies Permian strata including the Trold Fiord, Degerbols and Van Hauen formations. The contact is unconformable along the margins	Griesbachian
Smith Creek Member[2]	Medium to dark grey, silty shale with argillaceous siltstone interbeds common in the upper portion	320m thick	Occurs in northern Ellesmere and Axel Heiberg islands and along the eastern and southeastern margins; recognized in wells in the western Sverdrup Basin	Conformably overlies the Cape Butler Fm along the margins and conformably underlies the Pell Point Mbr	Dienerian to Smithian
Svartfjeld Member[2]	Medium to dark grey to black shale with siltstone interbeds in the upper portion	Few metres thick in marginal sections and up to 400m in basin centre	Mainly in the eastern and southeastern portions of the basin.	Along the margins, conformably overlies the Pell Point Member, and underlies the Cape O'Brien Member	Smithian to Spathian

Table 1.1: Official definitions of Lower Triassic formations and members (*1.* Christie et al., 1981; *2.* Embry, 1991)

distribution, age and suggested environment of deposition to sub-divide the Bjorne and Blind

Fiord formations into three members each, reflecting three major transgressive-regressive cycles.

The official nomenclature of the formations and members of the Lower Triassic are summarized

in Table 1.1 and discussed in Chapter 2.2. Sedimentological highlights were observed by

Devaney (1991), who described a broad facies assemblage over a large research area. The

assemblages suggested were sandy braided river, meandering river and marginal marine. This

thesis will reconsider the depositional environments, and provide greater context to the fluvial

system and style of sedimentation. While the Lower Triassic of the Sverdrup Basin is well

constrained, given the evidence published by Embry (regional thickness variations, facies

distributions, age relationships, sequence stratigraphy and paleogeography), it is lacking detailed

local facies studies, petrology, geochemisty and diagenetic timing.

1.4 Objectives

The research is a collaborative project with the Geological Survey of Canada, and is part of the Geo-Mapping for Energy & Minerals (GEM) project. This aim of the thesis is to provide a thorough account of the formation from one detailed section on Ellesmere Island and to contribute to understanding an important time of basin evolution by studying the depositional regime and diagenetic history. This thesis will address several topics:

1) The identification of facies associations will help create a depositional model for the Bjorne Formation and is the first step in understanding the shifting basinal environment and dominant depositional regime during rapid sedimentation in the Early Triassic.

2) Deposition took place immediately following the Permo/Triassic boundary. Extinction of many plant taxa at that boundary could have influenced fluvial styles because vegetation helps stabilize banks (Davies and Gibling, 2010). This thesis will explore whether the extinction event affected the depositional regime in the Early Triassic, or if at the time sedimentation began, sufficient roots and vegetation cover were present to bind sediment and influence the depositional style of the fluvial system.

3) There has been no research published on the petrology, diagenesis or geochemistry of the cement of the Bjorne Formation; this thesis will provide preliminary analyses of these subjects. Petrographic information will be used to formulate a model for burial history by looking at compaction, cementation and alteration. Thermal maturation, source rocks, seals and traps will be analysed, along with porosity data, to interpret the hydrocarbon potential within this unit. Sandstone reservoirs are relatively continuous with limited low permeability barriers.

CHAPTER 2: STUDY AREA AND STRATIGRAPHY

2.1 Study Area

The study area (Fig. 2.1) is located in the Sawtooth Range on Fosheim Peninsula, Ellesmere Island, Nunavut with the section of Bjorne Formation exposed along the flanks of a glacier and a glacial outwash stream. The base of the measured section is at 79°33.384N, 83°15.513W and the top at 79°33.926N, 83°20.907W. The outcrop was of variable quality. The exposure did not enable lateral variation in lithology to be observed, and a large portion of the middle sandstone member was very weathered, so minimal sedimentological data was recorded. The shale intervals of the Bjorne Formation were rubbly, covered intervals, and an igneous sill is present below the base of the measured section.

2.2 Stratigraphy
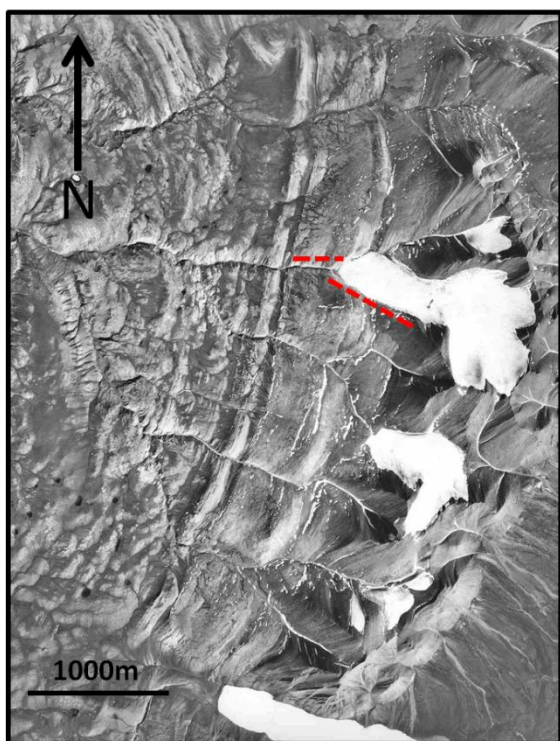
Figure 2.1: Airphoto of the study area in the Sawtooth Range, red line represents measured section.

The Bjorne Formation, along with the Blind Fiord Formation, is present across the majority of the Sverdrup Basin. The stratigraphic nomenclature of the formations (Fig. 2.2) reflects the occurrence of three major transgressive-regressive cycles in the Early Triassic of the Sverdrup Basin (Embry, 1986). The shale Smith Creek and Svartfjeld members can be classified as part of the Bjorne Formation along the margins of the basin, just as the sandstone units would be classified as members of the Blind Fiord Formation distally in the basin. The Lower Triassic strata accumulated in two

depocentres, the Fosheim and Melville segments (Fig. 2.3). The two depocentres maintained their position and subsided rapidly, and thus there was little basinward progradation in spite of the high sediment supply (Embry, 2009).

In the Sawtooth Range, the Bjorne Formation is underlain by the Middle Permian glauconitic shoreface sandstone, the Trold Fiord Formation. It is unknown if the Cape Butler Member or the Confederation Point Member of the Blind Fiord Formation unconformably overlies the Permian sandstone because it is covered in rubble (Fig. 2.4). Overlying the Bjorne Formation is dark organic-rich mudstone and siltstone of the Middle Triassic Murray Harbour Formation which signalled a basin wide transgression with the sediment supply drastically decreased. The Lower Triassic succession in the Canadian Arctic represents the base of the Triassic system because ammonite-bearing beds have been correlated to the *Otoceras woodwardi* Zone of the Himalayas (Nassichuk et al., 1973), traditionally taken to define the base of the Triassic System.

The outcrop measured in the study area totalled approximately 1,000 m in thickness (Fig. 2.5). The basal member (Cape Butler) is 240 m, the middle member (Pell Point) is 280 m, and the topmost member (Cape O'Brien) is 300 m thick. The shale tongue (Smith Creek Member), between the Cape Butler and Pell Point members, is 120 m thick, but was entirely covered interval. The percentage of covered interval in each member is 19%, 1% and 34%, respectively. The percentage of sandstone to shale when observing the lithology in each member is approximately 88%, 98% and 100%. If the covered intervals in each member represent recessive shale, the ratio of sandstone to shale becomes approximately 69%, 97% and 66% which shows a substantial dissimilarity in both the oldest and youngest members when compared to the ratios derived from solely outcrop lithology.
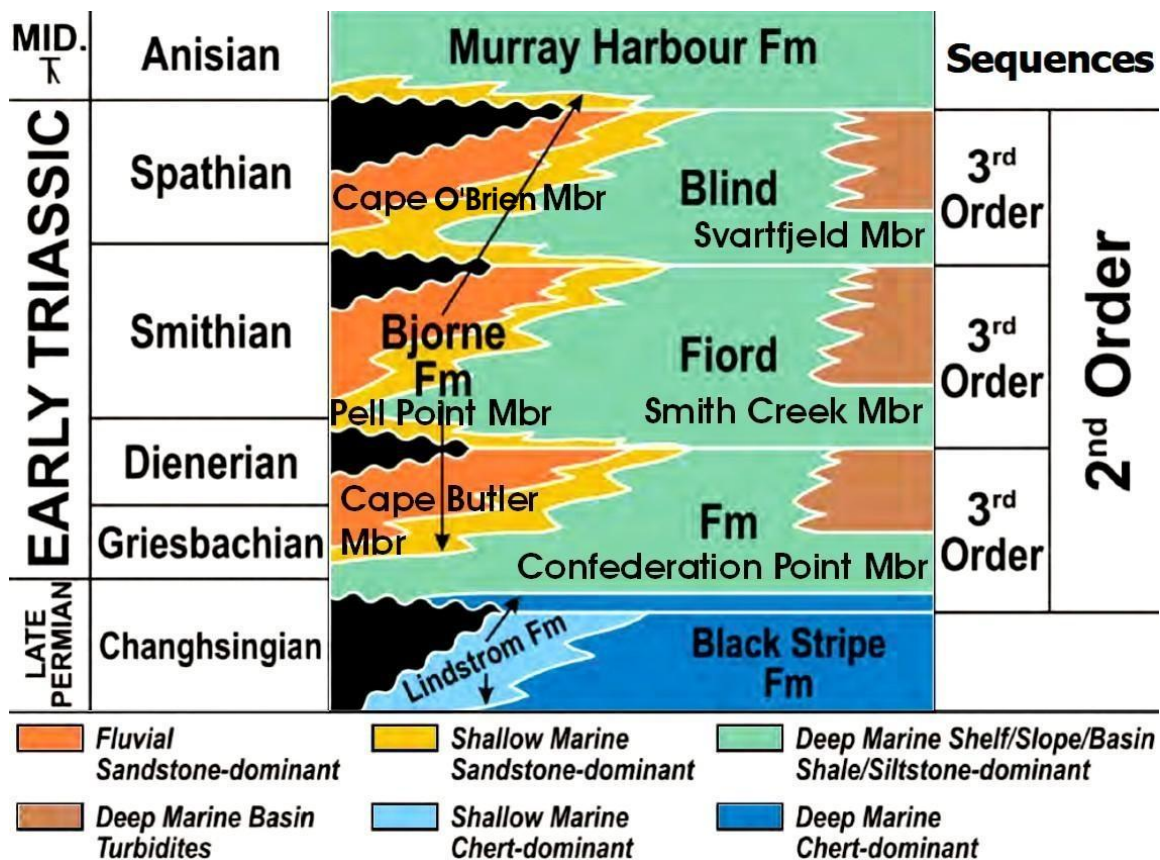
Figure 2.2: Stratigraphic column of the Lower Triassic Bjorne and Blind Fiord formations with sequence stratigraphy (modified after Embry, 2009).
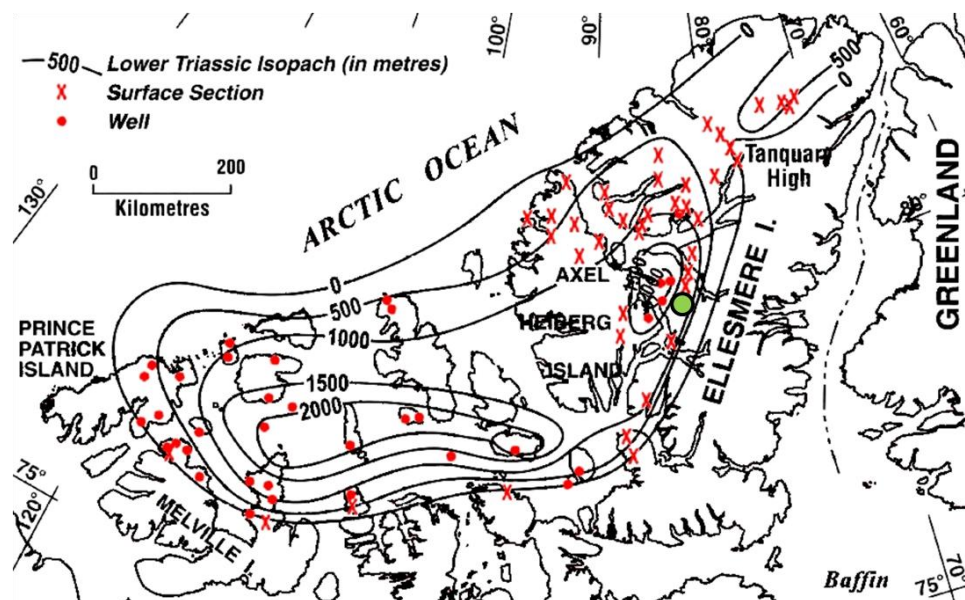
Figure 2.3: Isopach map of the Lower Triassic displaying wells and surface sections, the Melville depocentre is on the southern margin, and Fosheim is on the eastern margin. Green circle represents study area (modified after Embry, 2009).
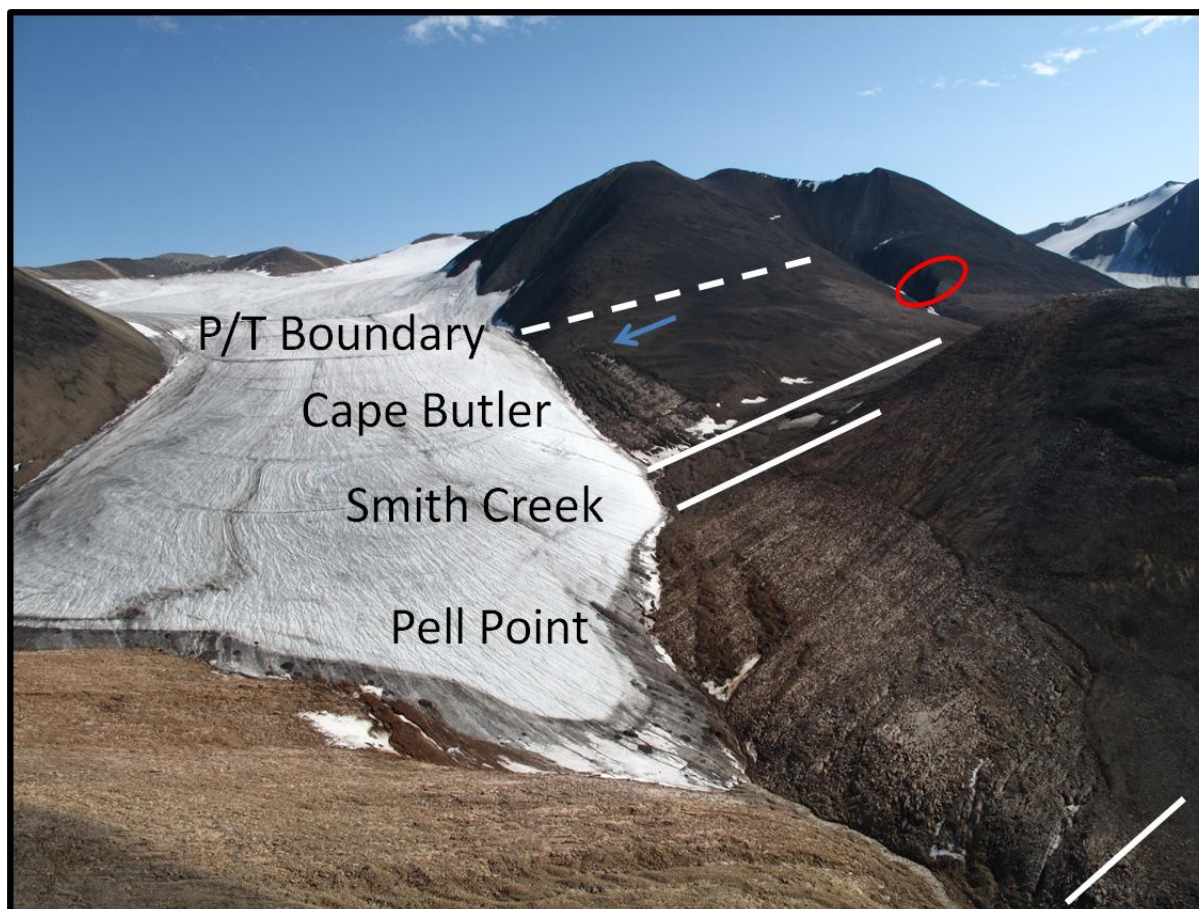
Figure 2.4: Aerial photograph of the study area in the Sawtooth Range. Outcrop decreases in age to the bottom of photo. P/T Boundary is estimated, Cape O'Brien is present off-photo; photo scale is variable, Cape Butler (240m), Smith Creek (120m), Pell Point (280m); Blue arrow represents base of measured section; Red circle represents location of igneous sill.

    The start of the measured section was the first exposed sandstone/siltstone bed in the rubble, so it likely does not represent the base of the Bjorne Formation, and is assumed that the outcrop represents the Cape Butler Member rather than the marine Confederation Point Member. Figure 2.4 shows the measured section with contacts, and location of the sill and base of measured section. The contact definition between the two members is placed at the base of the first sandstone above which sandstone in predominant (Embry, 1986). This may be difficult to determine with the amount of covered interval at the base of the section. Given the high elevation of the Permian strata, the rubble has moved downslope to cover the lower Bjorne Formation, as seen in the first 70 m of the section which was largely covered interval with the
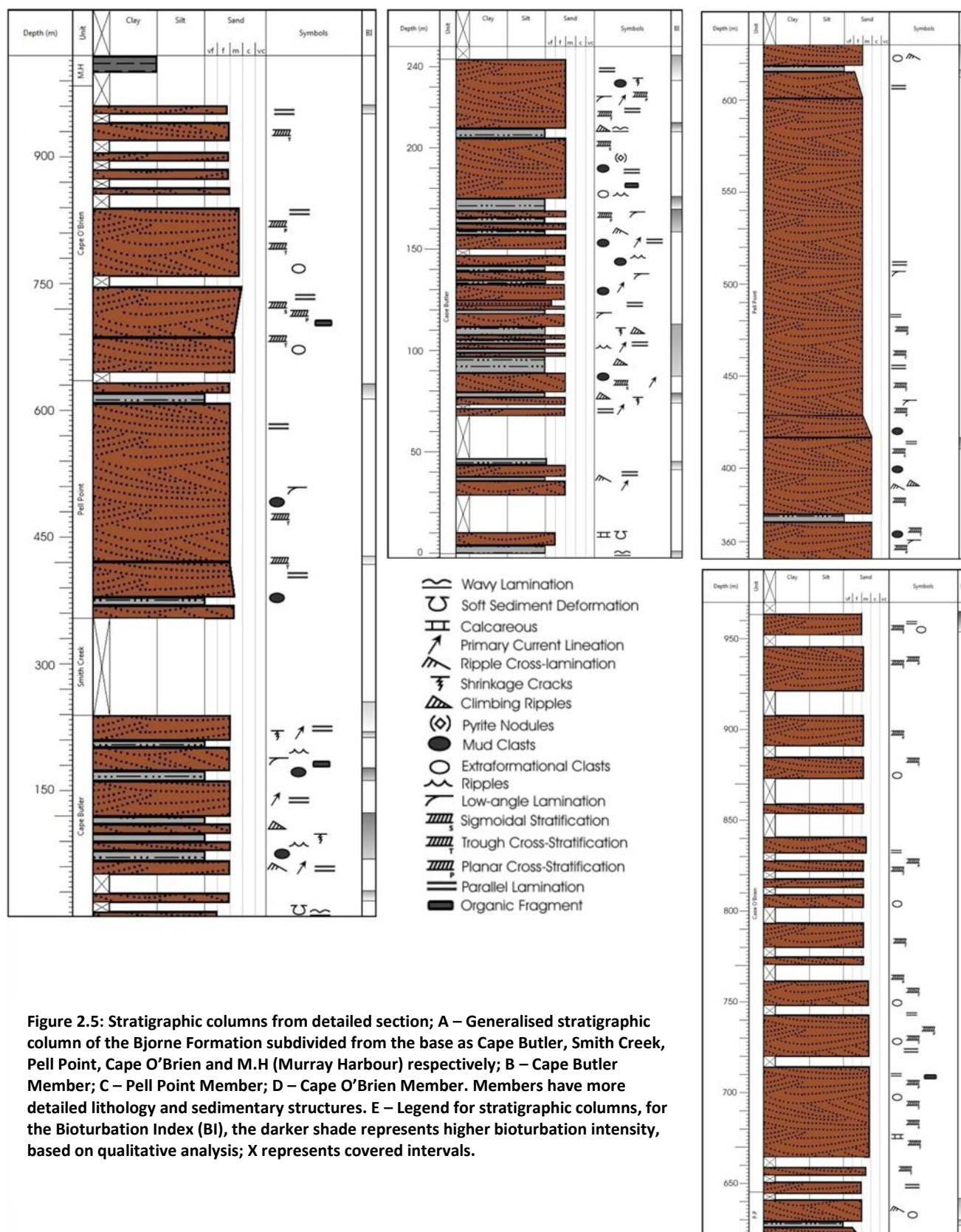
Figure 2.5: Stratigraphic columns from detailed section; A – Generalised stratigraphic column of the Bjorne Formation subdivided from the base as Cape Butler, Smith Creek, Pell Point, Cape O'Brien and M.H (Murray Harbour) respectively; B – Cape Butler Member; C – Pell Point Member; D – Cape O'Brien Member. Members have more detailed lithology and sedimentary structures. E – Legend for stratigraphic columns, for the Bioturbation Index (BI), the darker shade represents higher bioturbation intensity, based on qualitative analysis; X represents covered intervals.

rubble being made up of the Trold Fiord Formation containing abundant brachiopods and *Zoophycos*. These have been dated from other sections with the highest Permian unit being early Guadalupian, or Middle Permian (Nassichuk et al., 1973). After 70 m, the rubble was predominantly sandstone from the Bjorne Formation. An igneous sill was observed on a river cut at 79°32.921N, 83°16.172W, away from the measured section, with the Bjorne Formation overlying, and Trold Fiord Formation underlying.

The Cape Butler and Pell Point members are separated by the shale tongue of the Smith Creek Member, represented by an erosional gulley. The contact between the two sandstone members and the Smith Creek Member is placed when sandstone becomes the dominant lithology.

The contact between the Pell Point and Cape O'Brien members is less clear landward, as the Svartfjeld Member thins and eventually pinches out. This creates an erosional unconformity between the two sandstone members. The contact was picked at a covered interval above a bioturbated surface at the top of the Pell Point Member. It is thought that the transgression occurred in association with the presence of bioturbation, and the next pulse of sand is represented by the Cape O'Brien Member, which overlies the covered interval. Although the sedimentology is similar to the Pell Point Member, the grain size is slightly coarser with a slight variation of facies distribution.

Given that the Bjorne Formation is Early Triassic in age, the measured section had been designed to include the Permian-Triassic boundary; however, given the poor exposure, the boundary was buried in the rubble and unobservable. Both physical and paleontological evidence points toward a hiatus in sedimentation between the Permian and Triassic of Arctic Canada along the margins of the basin (Nassichuk et al., 1973). Although there is no hiatus in the axial, deeper

part of the Sverdrup Basin with the Upper Permian and Lower Triassic succession being conformable, the margins of the basin shows a major sub-Triassic unconformity.

The basal Blind Fiord Formation contact coincides with the Latest Permian Extinction, which is marked by an abundance of pyrite, a trait of the extinction horizon around the world, and conformably overlies the Late Permian Lindström and Black Stripe formations (Beauchamp et al., 2009). Algeo et al. (2012) disagreed with the interpretation by Beauchamp et al. (2009) of the contact between the Blind Fiord and Lindström formations, as they consider that the contact represents the Arctic Extinction Event, which predates the latest Permian mass extinction. The stratigraphic correlation framework developed by Algeo et al. (2012) suggests that the Permian-Triassic boundary is ~13 m above the base of the Blind Fiord Formation at West Blind Fiord, with an uncertainty of about ±5 m, with the Latest Permian Extinction placed ~5.6 m above the base. West Blind Fiord is on southern Ellesmere Island, approximately 160 km to the south-southwest, and represents a more distal setting in the Sverdrup Basin than in the Sawtooth Range where the Triassic and Permian strata are conformable. This importance of the extinction events and their age proximity to the Lower Triassic strata will be elaborated in Section 6.1.

The proximity in time of the Bjorne sands to the Permian-Triassic extinction event could have some importance in the characteristics of the depositional environment. The lack of fauna from late Permian time, and the correspondence of the basal Triassic beds with the defined base of the Triassic System, indicates that the break in sedimentation along the margins lie entirely within the Permian.

CHAPTER 3: METHODS

3.1 Field Data Collection

The time spent in the field was two weeks in early July, 2011 with several days of logistics planning in Resolute, NU, facilitated by the Polar Continental Shelf Program (PCSP). A base camp was run out of Eureka, a high-Arctic weather station and seasonal military base. The base camp provided support for field work. To perform the research, a PCSP helicopter transferred the gear to the Sawtooth Mountain Range approximately 80 km southeast of Eureka; field work was conducted out of a fly camp for four days. A global positioning receiver (GPR) was used to collect co-ordinates at the start and end of each traverse, and an aerial photo was used in conjunction with the GPR to find the relative position during the traverse. A 1.5 m pogo stick was used to measure the thickness of the unit. Throughout the measured section, photographs were taken abundantly to accompany the notes and qualitative descriptions were taken from observations. Paleoflow was measured using primary current lineations, which were principally in the lowermost member; any cross stratification was not used for paleocurrent analysis as it was not exposed in three dimensions. A large number of samples were collected for further petrographic analysis; however, the samples were not taken at systematic intervals, but were collected to display the varying facies or lithology changes to document any potential trend over the entire Bjorne Formation or individual members. Given the thickness of the outcrop and the available time to map, the level of detail for the measured section was done on the scope of reconnaissance mapping; therefore, the level of interpretation is bound to be generalized.

3.2 Stratigraphic Column Illustration

In order to plot up the sections for graphical representation, the program PSICAT (Paleontological Stratigraphic Interval Construction and Analysis Tool) was used. PSICAT is a graphical editing tool using Java, for creating stratigraphic columns from outcrop data. It allows

the user to customize the task of working with stratigraphic columns and captures data digitally

as the diagram is prepared. Further customization and illustration was required to produce a

polished figure. The program used was Corel Photo-Paint, a raster graphics editor.

3.3 Lithofacies Classification

In order to conduct facies analyses from the data collected from the field, a systematic method

for classification was needed. Miall (1996) created such a methodology by using different

components of primary deposition, principally bedding, grain-size, texture and sedimentary

structures. Biogenic structures and chemical sediments provide additional descriptive

characteristics. The two-letter code system for lithofacies applies to all fluvial deposits and is the

standard field methodology for description of fluvial deposits. Miall (1990) noted that the scale

of a particular lithofacies unit can be defined broadly or finely depending on the level of detail

appropriate for the study. In this case, the research was reconnaissance level mapping, so the

facies interpretation is a broad representation of the measured section.

3.4 Petrographic Studies

Most of the samples were cut for thin-section with the exception of a few delicate samples

displaying trace fossils. Thin-sections are mostly from the Bjorne Formation and its respective

members, but also include a sample from the Murray Harbour Formation. From the 23 samples

taken, 21 thin-sections were cut and polished at the Dalhousie University thin-section

preparation facility by Gordon Brown. An individual work sheet was filled out for each thin

section with a list of grain types, features and a percentage of components estimated using

qualitative analysis. This data was subsequently used to create triangular diagrams, but excluded

thin sections taken from siltstone. A summary of the modal percentages from work sheets are

placed in Appendix B. The ternary plots were produced by TernPlot, a program which uses Microsoft Excel and were polished afterwards using CorelDraw.

Three thin sections, one from each member of the Bjorne Formation, were mounted with blue epoxy to highlight porosity. Point counting was used to quantitatively measure porosity; the slides were scanned, then the image was inserted into CorelDraw and overlain by a continuous grid system with each grid square being .067 mm in length. The limitation of this method is both the resolution of the photo, and the identification of pore space. The margin of error was not determined on the porosity and modal percentages, but with approximately 300 counts per slide, this will provide an accurate estimation of porosity.

3.5 Electron Microprobe

Two thin sections were used for electron probe microanalysis in the lab at Dalhousie University operated by Dan MacDonald. The probe determines the composition of specific spots on a mineral. Each thin section is carbon-coated in order for electrons to be conducted away after striking the sample. The methodology is described in detail by Nesse (2000), and is summarized here. A continuous spectrum is produced by a beam of electrons striking the sample, with some electrons losing their energy by hitting atoms in the sample. Each of the different elements in the sample emits a characteristic spectrum, with the abundance of an element in a mineral sample based on the intensity of the distinguishing X-ray spectrum for a given element. In order for an accurate spectrum to be provided, the microprobe needs to be calibrated for a known composition. X-rays coming into the sample are diffracted by a diffracting crystal with a known d spacing; the crystal is arranged at angle θ from the Bragg Equation ($n\lambda = 2d \sin\theta$). The microprobe analysis was used primarily for the elemental composition of minerals and carbonate cements. The operating conditions were 15 kV, and the elements used for analysis were K, Cr,

Na, Si, Mn, Ca, Ti, Mg, Al, Fe and Ba. The tables of geochemical data are located in Appendix

C. The size of the beam used was 1 μm.

3.6 Sediment Flux

Sediment flux rates were calculated using linear sedimentation rates (LSR) for a time-stratigraphic unit of interest (i.e., the Changhsingian, Griesbachian or Spathian) based on its thickness at the study site and its estimated duration; for the analysis, ages are the same used by Algeo et al. (2010). The following equations and methods are the same to those used by Algeo et al. (2010); linear sedimentation rates were calculates as: $LSR = \varphi / \tau$ where φ is thickness in units of meters (m), and τ is duration in units of millions of years (Myr.); bulk accumulation rates (BAR) were calculated as: $BAR = LSR \times \rho$ where BAR is in units of $g\ m^{-2}\ yr^{-1}$, LSR is in units of m/ Myr, and ρ is bulk sediment density in units of $g\ cm^{-3}$. Owing to lack of bulk sediment density data, a value of $2.5\ g\ cm^{-3}$ is used in all BAR calculations.

3.7 Trace Fossils

Identification of the trace fossils were made with the assistance of Lynn Dafoe of the GSC Atlantic by using a few samples and photographs from the field.

CHAPTER 4: SEDIMENTOLOGY, ICHNOLOGY, AND LITHOFACIES INTERPRETATION

4.1 Lithofacies Description

4.1.1 Cape Butler Member

The Cape Butler succession is composed primarily of strata deposited under conditions of the upper flow regime or the transition to the lower flow regime. The unit is composed of fine- to medium-grained sandstone and sandy siltstone. The sand beds display no discernible variation in upward grading or lateral grain-size changes, and bedding thickness ranges from 5 cm to 50 cm. Horizontally stratified sandstone facies (Sh) commonly displays primary current lineation, and is the most abundant facies. Examples of lithofacies in the Bjorne Formation are in Figure 4.1, with many of them interpreted as upper flow or the transition to the lower flow regime. Primary current lineation, also known as parting lineation, is the result of microvortices acting under high flow rates to sort and deposit sand grains and can be used to measure paleocurrent as it is formed parallel with direction of current flow (Picard and High, 1973). Only three measurements were taken for paleoflow, with values of 188°, 222°, and 258°; they were estimated by direct sighting on the dipping surface. Primary current lineation is a bipolar structure, and paleocurrent orientation is assumed after comparison with associated cross-strata, which could not measured be precisely, but indicate a general dip direction towards the west to southwest.

Low angle and sigmoidal stratified sandstone facies (Sl) represents the transitional regime and is the next most abundant facies. As the dune-upper plane bed transition is approached with increasing flow velocity, dune cross-sets change from a concave-upward to a sigmoidal geometry with preserved topset, foreset and bottomset elements (Fielding, 2006). Planar (Sp) and trough (St) cross-stratified sandstone facies are less common and represents lower flow power than Sh and Sl, and were not observed in the lower part of the member.
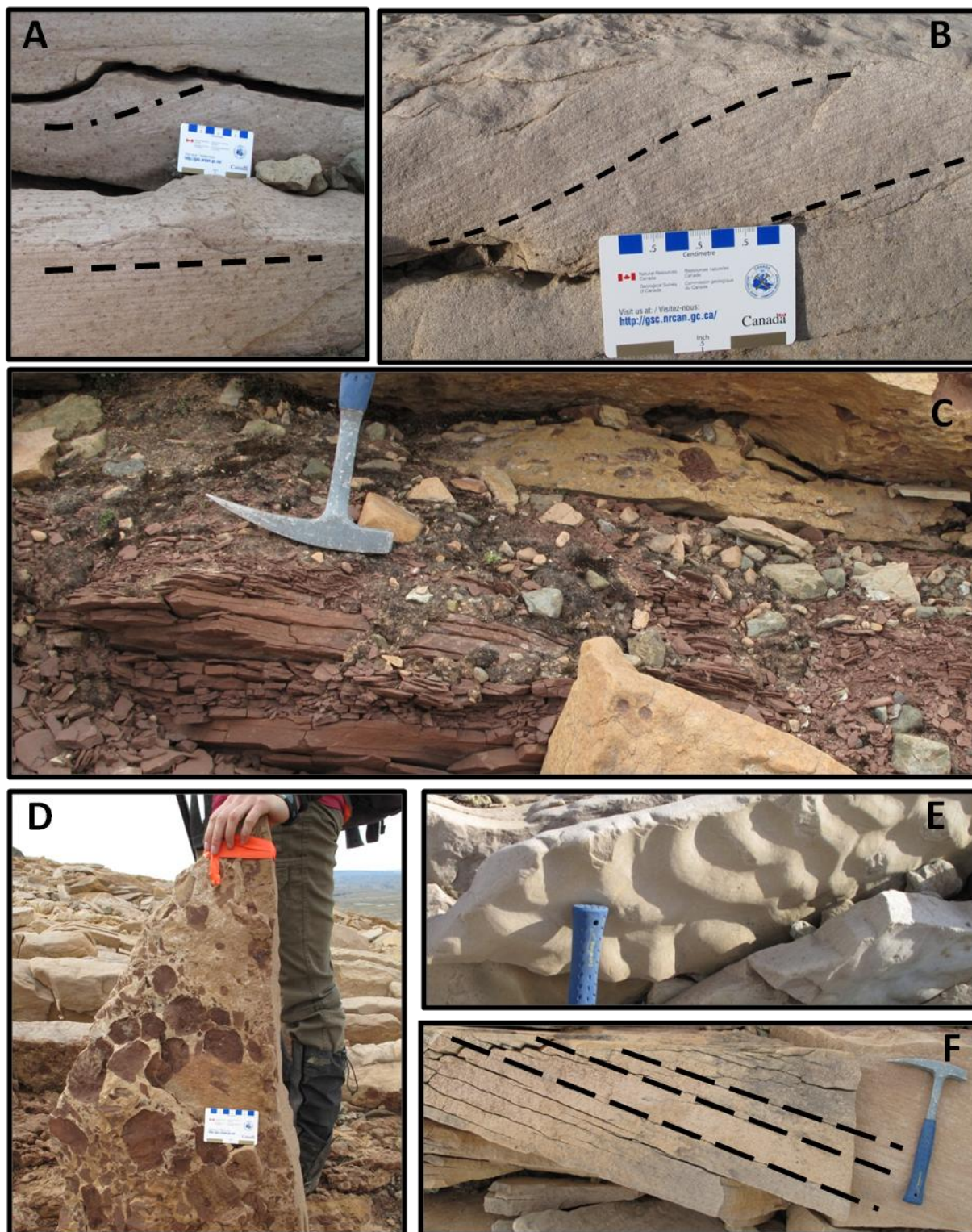
Figure 4.1: Lithofacies of Bjorne Formation. A – Facies Sh (bottom) and St (top), upper Cape Butler Mbr; B – Facies Sl with sigmoidal (left) and low angle (right) stratification, upper Cape Butler Mbr; C – Facies Fl, massive red siltstone, Pell Point Mbr; D – Facies Se showing rip-up clasts, Pell Point Mbr; E – Facies Sr, with linguoid ripples, top of bedding surface, upper Cape Butler Mbr; F – Facies Sp, Pell Point Mbr; Hammer is 30cm long, and 15cm wide; GSC scale card – 8 cm long.

At the base of the sandstone units are erosional scours with mud- to siltstone intraclasts (Se). The scour surfaces are concave-up, but vary from prominent, high-relief features to predominantly gentle, low-relief features. The red, sub-rounded intraclasts commonly range from 1 mm to 1 cm in diameter, and have no preferred orientation. This facies is ubiquitous when overlying a siltstone bed, but can also occur when no silt underlies a sand bed. The tops of sandstone units have rare ripple cross-stratified sands (Sr), usually in the form of preserved linguoid ripples (Fig. 4.1E). More commonly, the top of the sandstone has vertical and horizontal trace fossils preserved as well as a thin silt veneer, which is more prominent in the lower part of the member.

Red sandy siltstone beds with ripple cross lamination (Fl) are sharply overlain and underlain by the sandstone units. This facies ranges from 30 cm to 4 m in thickness. There are climbing ripples present, Type B – depositional stoss as defined by Allen (1973). These are characteristic of ripple migration rates being less than aggradation rates, allowing for the preservation of the stoss slope. Type B has comparatively higher rates of aggradation than type A – erosional stoss. In one case, the climbing ripples appear to gradationally change towards the classification of draped lamination. Trace fossils are preserved and are more abundant in the upper part of the bed with the bioturbation disturbing the sedimentary features. On a few bedding surfaces, shrinkage cracks were observed in plan view, but no cross sections of the cracks were seen.

The distribution of these sedimentary structures, facies and bioturbation are not uniform throughout the member and can be represented in terms of an upper and lower separation. The lower unit of the Cape Butler Member has a higher abundance of fine-grained sandstone-siltstone beds along with bioturbation and shrinkage cracks. Given the lesser grain size, the lower unit lacks the lithofacies St and Sp, so it is deficient in dune structures. The Cape Butler
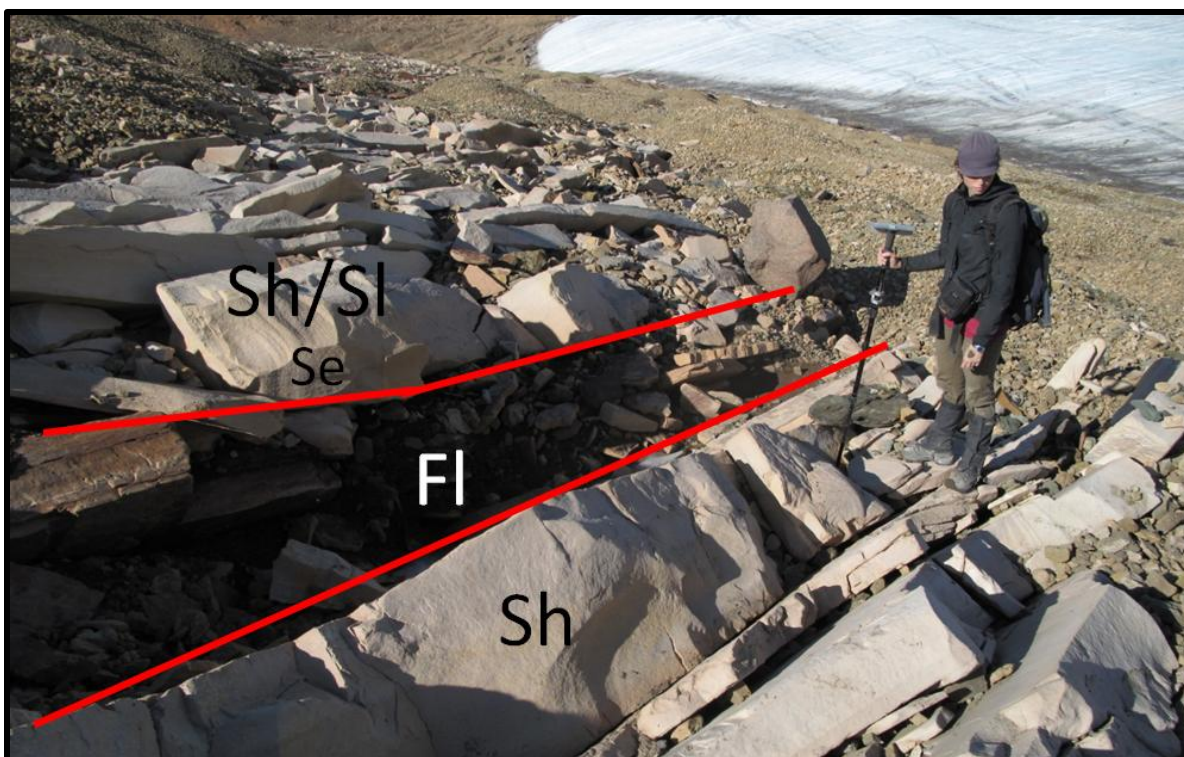
Figure 4.2: Typical outcrop in Cape O'Brien Member, displaying common lithofacies in the ephemeral sand sheet fluvial system, Sh, Sl, Se and Fl. Measuring pole is 1.5m.

Member is composed primarily of upper flow regime plane beds that display rapid transition to lower flow regime bedforms, mainly ripples. Trough cross-beds formed by dunes are scarce in the upper part and thin red siltstones cap some waning-flow successions. A typical succession of the Cape Butler Member (Fig. 4.2) is lithofacies Sh and Sl capped by Fl, overlain by Se, Sl and Sh at the base of the next sandstone unit; St and Sp is present solely in the upper part of the member. Additional structures include bedforms in the upper/lower regime transition, antidune bedding, humpback cross-bedding, one possible chute-and-pool structure, and many erosional surfaces, many of which are lagged with mudstone intraclasts. Soft-sediment deformation occurs at the base of the member. The chute-and-pool structure is subject to some debate given its rare preservation; alternatively, it represents an unusual erosional scour from high flow.

4.1.2 Pell Point Member

The facies codes described in the previous section will not be elaborated on further, unless to highlight changes. This succession is similar to the Cape Butler Member, as it is composed of strata deposited under conditions of the upper flow regime or the transition to the lower flow regime; however, the middle Pell Point Member is dominated by dune cross-stratification, with some parallel lamination. The unit is composed of fine- to medium-grained sandstone, but sandy siltstone is only represented by two 2 m beds. The sandstone beds typically range from 10 cm to 75 cm in thickness, and display a lack of variation in upward grading or lateral grain-size changes. The majority of the exposed outcrop was affected by the occurrence of Liesegang bands (Fig. 4.3A), making it difficult to assess the sedimentary structures present. Liesegang banding appears after deposition, compaction and cementation, and normally cross-cut stratification and lamination; discrete bands of iron hydroxide form from water-rock interaction causing nucleation and crystal growth (Steefel, 2008).

Apart from the lack of siltstone, the Pell Point Member is fairly similar to the Cape Butler Member in terms of the facies presence. Pell Point Member is made up of facies Sh, Sl, Sp, St, Se and Sr, but Sr is very rare, and Se is present in the lower portion of the member and absent after approximately the first 100 m. The mud clasts are larger than in the previous member with a maximum diameter of 8 cm (Fig. 4.1D). Sh is present, but no parting lineation was observed in this member. There is one bedding surface with trace fossils which is underlain by a bed with abundant siltstone clasts. The member displays fining upward successions approximately 5 m thick, beginning with the predominant facies in the member, St or Sp at the base, with Sl and transitioning into facies Sh, capping the succession.

Figure 4.3: A – Liesegang banding, Pell Point Mbr; B – Plant fragment, Cape O'Brien Mbr; C – Herringbone cross-bedding, Cape O'Brien Mbr. D – Extra-formational clasts, Cape O'Brien. Hammer is 30 cm long and 15 cm wide, notebook is 20 cm long, pen is 12 cm long.
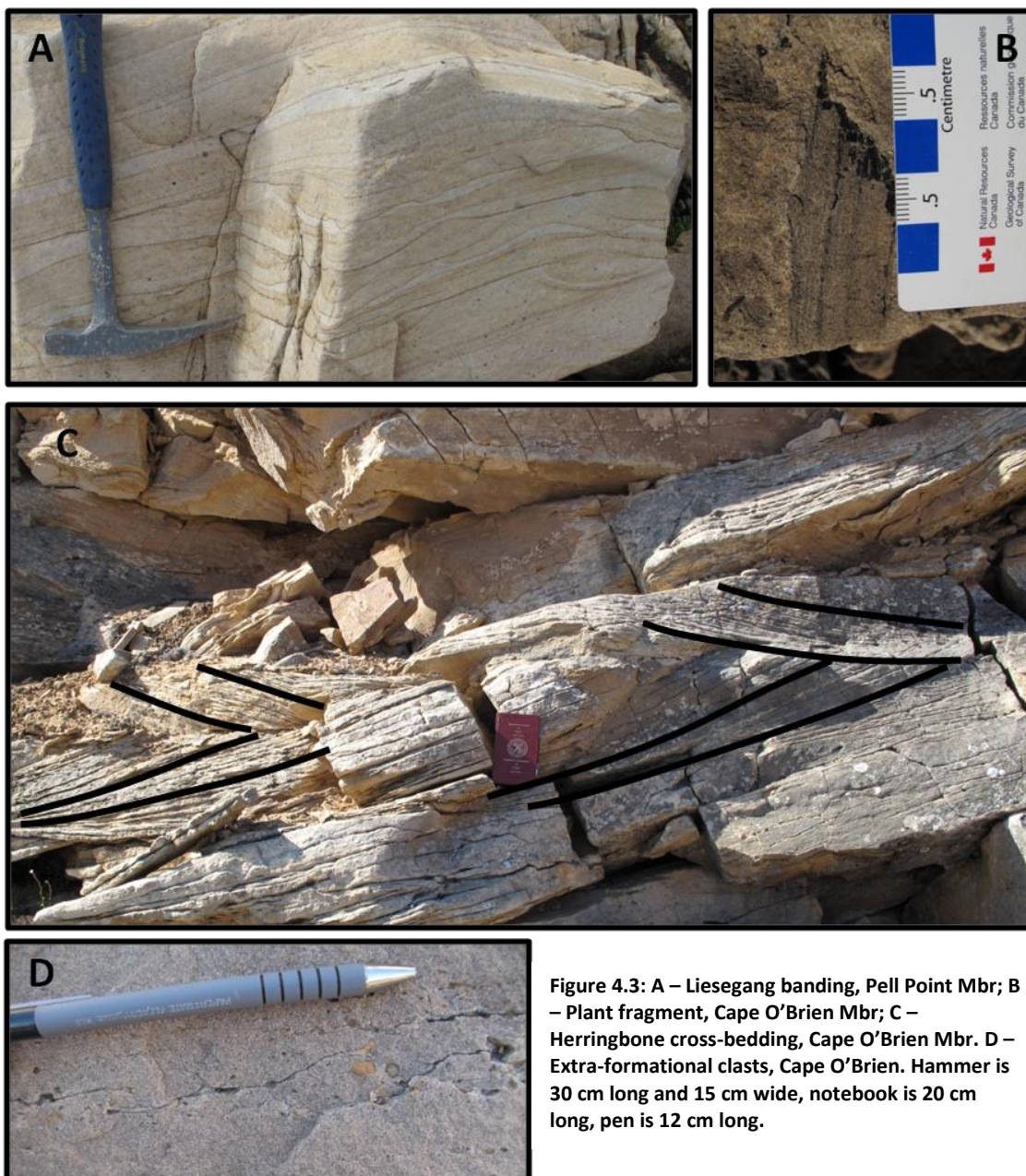
4.1.3 Cape O'Brien Member

The Cape O'Brien Member is composed of fine- to medium-grained sandstone, with red, sandy siltstone not appearing in outcrop. In the upper portion of the member, there are frequent covered intervals and the outcrop quality was generally poor and rubbly. The member is similar to Pell Point, with a large occurrence of dune cross-stratification. Herringbone cross-bedding (Fig. 4.3C) was observed at the base of the member in approximately 30 cm sets. Rare wood fragments were observed (Fig. 4.3B), and rather than intraformational mud rip-up clasts present,

scattered extra-formational clasts were common throughout the member in discrete bands; however, not always above an erosional surface (Fig. 4.3D). The clasts are very-fine to fine gravel and the predominant lithology is quartzite with lesser limestone and granitic clasts. Facies Fl, Sr and Se were not observed. At the top of the member, a succession of pebble lags underlying cross-stratified beds and overlying planar-laminated beds was repeated over 5 m. Similar to the Pell Point Member, facies St, Sp and Sl are more abundant than Sh, representing slightly lower flow power than for the Cape Butler Member.

4.2 Bioturbation

Trace fossils are present in all members with most occurring in the lower unit of the Cape Butler Member. The trace fossils are mostly restricted to bedding surfaces, commonly at the top of a siltstone bed or on sandstone underlying a siltstone bed or covered interval. The assemblage consists of *Thalassinoides, Diplocraterion, Skolithos, Planolites, Scoyenia, Paleophycus, Psilonichnus* and *Arenicolites* (Fig. 4.4).

In rapidly flowing streams there is minimal likelihood that biogenic structures will be preserved as the predominant surficial traces will be eroded (Miller, 1984). As the current decreases and more sediment falls out of suspension, the probability of preservation increases. Burrowing intensities tend to decline in response to high sedimentation rates; this will limit the range of ichnofossils as the (re)colonization of the substrate is challenging and can limit the ability of organisms to reposition borrows following sediment accumulation (MacEachern et al., 2010). Low bioturbation intensity relates to high sedimentation rates, and given the episodic nature of the sedimentation, organisms might be able to thrive briefly after deposition wanes.

The following information about trace fossils and ichnofacies are from Pemberton et al. (2001). *Thalassinoides*, found in lower shoreface to offshore environments as well as low

Figure 4.4: Trace Fossils in the Bjorne Fm, A – *Thalassinoides* **and** *Planolites* **(Circled), lower Cape Butler Mbr; B –** *Arenicolites* **and** *Planolites***, small dots are patches of lichen, not burrows, lower Cape Butler Mbr; C –** *Skolithos* **or** *Psilonichnus***, upper Cape Butler Mbr; D –** *Skolithos***, Cape O'Brien Mbr; E –** *Diplocraterion***, Pell Point Mbr. A, C and E are on bedding surfaces; hammer is 30 cm long, 15 cm wide.**

diversity, brackish-water suites, is part of the *Cruziana* ichnofacies and appears with *Planolites* (Fig. 4.4A), found in virtually all environments from freshwater to deep marine. *Arenicolites* (Fig. 4.4B) was observed in one outcrop and is generally associated with arenaceous substrates in low energy shoreface or sandy tidal flats, but is more abundant in brackish-water settings than marine. *Psilonichnus* (Fig. 4.4C) variably represents marine and non-marine conditions, and *Skolithos* (Fig. 4.4D) is indicative of relatively high levels of current energy, and typically is developed in clean, well-sorted, loose or shifting particulate substrates. *Skolithos* is common where there are abrupt changes in rates of deposition, erosion and physical reworking and can be constructed by many kinds of organisms and found in virtually every type of environment from marine to non-marine (Pemberton, 2001). *Diplocraterion* (Fig. 4.4E), part of the *Skolithos* ichnofacies, is common on sandy tidal flats and in estuarine channel deposits.

As observed in the measured section, some beds are thoroughly bioturbated, perhaps with a monospecific trace-fossil assemblage, whereas closely adjacent beds are non-bioturbated; such fluctuation may be seasonal in nature due to variations in river discharge that lower salinity and/or increase the sedimentation rate (Dalrymple and Choi, 2007). While the assemblage of trace fossils indicates a marine influence, it is not indicative of a specific depositional environment.

4.3: Lithofacies Interpretation – Ephemeral Braid-Delta

Given the reconnaissance level of mapping, interpretations must be considered preliminary. The three members appear to have depositional systems with predominant flow in the upper flow regime and the transition to the lower flow regime. The regime is based on the Froude number which is governed by velocity and depth as critical factors. The Froude number may exceed 1.0 if depth decreases at a constant velocity, or when velocity increases at constant depth. The
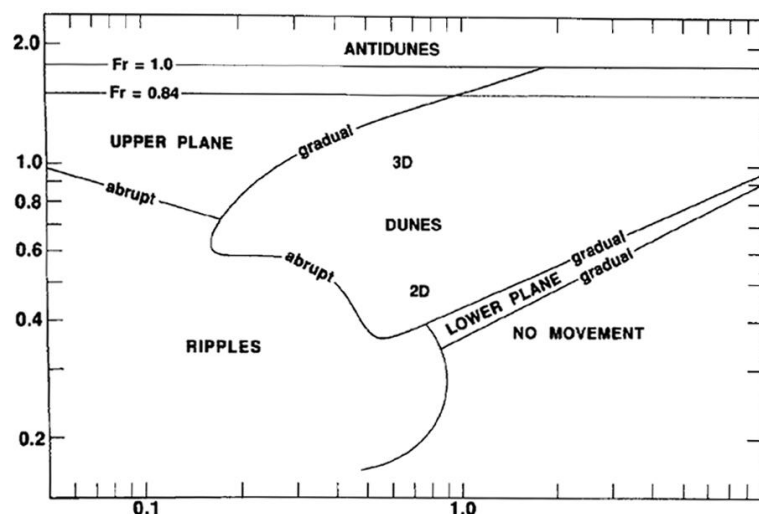
Figure 4.5: Plot of mean flow velocity against mean sediment size showing the stability of fields of bed phases. Fr= Froude number (from Southard and Boguchwal, 1990).

succession of sedimentary structures with increasing Froude Number depends on the grain size (Fig. 4.5).

The sedimentary structures may appear comparable in each member, but there is a clear distinction that deposition did not occur entirely in the same depositional environment. With two lithologically different types of units, as shown in Figure 4.2, facies Sh, Sl, Se, Sp, St and Sr can be grouped as multi-story channel sands and facies Fl and Sr as fine-grained deposits formed from episodic flooding events or from channel abandonment. The multi-story and heterogeneous character of the sandstone bodies suggests repeated occurrences of channel scouring and deposition (Røe and Hermansen, 1993). The abundance of upper flow regime features is seen in the predominance of horizontally and low angle stratified deposits which fill erosional troughs in multi-story sand sequences; collectively, these features indicate ephemeral flow conditions (Stear, 1983). There are several indications of highly variable flow power, with a rapid transition from high power to waning flow. In particular, for facies Se, the abundance of rip-up clasts is a typical feature of ephemeral deposits because during waning flow, finer sediment will accumulate in abandoned channels. As renewed flood events occur, mud will be removed as the channel is scoured and clasts will form. Along with the presence of rip-up clasts, the abundance of broad, erosional surfaces provides further evidence for the high

energy of the system in which rapid, episodic discharges continually scoured the alluvial surface (Rust, 1984).

The absence of coarser sediment or conglomerate units does not necessarily imply that flow rates were modest during deposition of the Bjorne Formation. A type example of ephemeral, sheet-flood, sand-bed fluvial systems is derived from Bijou Creek described by McKee et al. (1967). In Bijou Creek, a maximum of about 4 m of fine-grained sand was deposited from one flooding event along with steel girders from a bridge. Even though the flow rate was high, the sediment grade available was fine-grained sand, so the sediment deposited was a function of the maximum size of sediment particles available. This is the case for the Bjorne Formation which is sourced mainly from Devonian siliciclastics of a predominant sand grade (Patchett et al., 2004), and thus regardless of the velocity of the ephemeral flooding events, the maximum grain size will not reach pebble- or cobble- sized grains with the exception of the few extraformational clasts.

There are some uncommon bedforms that are representative of transitional to upper flow regime beds (Fig. 4.6A). Fielding (2006) outlined several from ancient fluvial successions which indicate sediment accumulation under the influence of episodic and pronounced flooding events. The first is humpback cross-bedding, a combination of sigmoidal to low-angle stratification that is interpreted as the transition from dune to upper plane bed conditions (Røe and Hermansen, 1993). The preservation of these structures in predominantly horizontally stratified sandstone implies fluctuating conditions, and once upper plane bed conditions are achieved, planar lamination, along with primary current lineation, is the predominant bedform (Fig. 4.6C). Antidunes (Fig. 4.6B) form in the transition from upper plane bed to antidune stability fields. There is also an unusual feature that resembles chute-and-pool structures (Fig. 4.6D); this feature
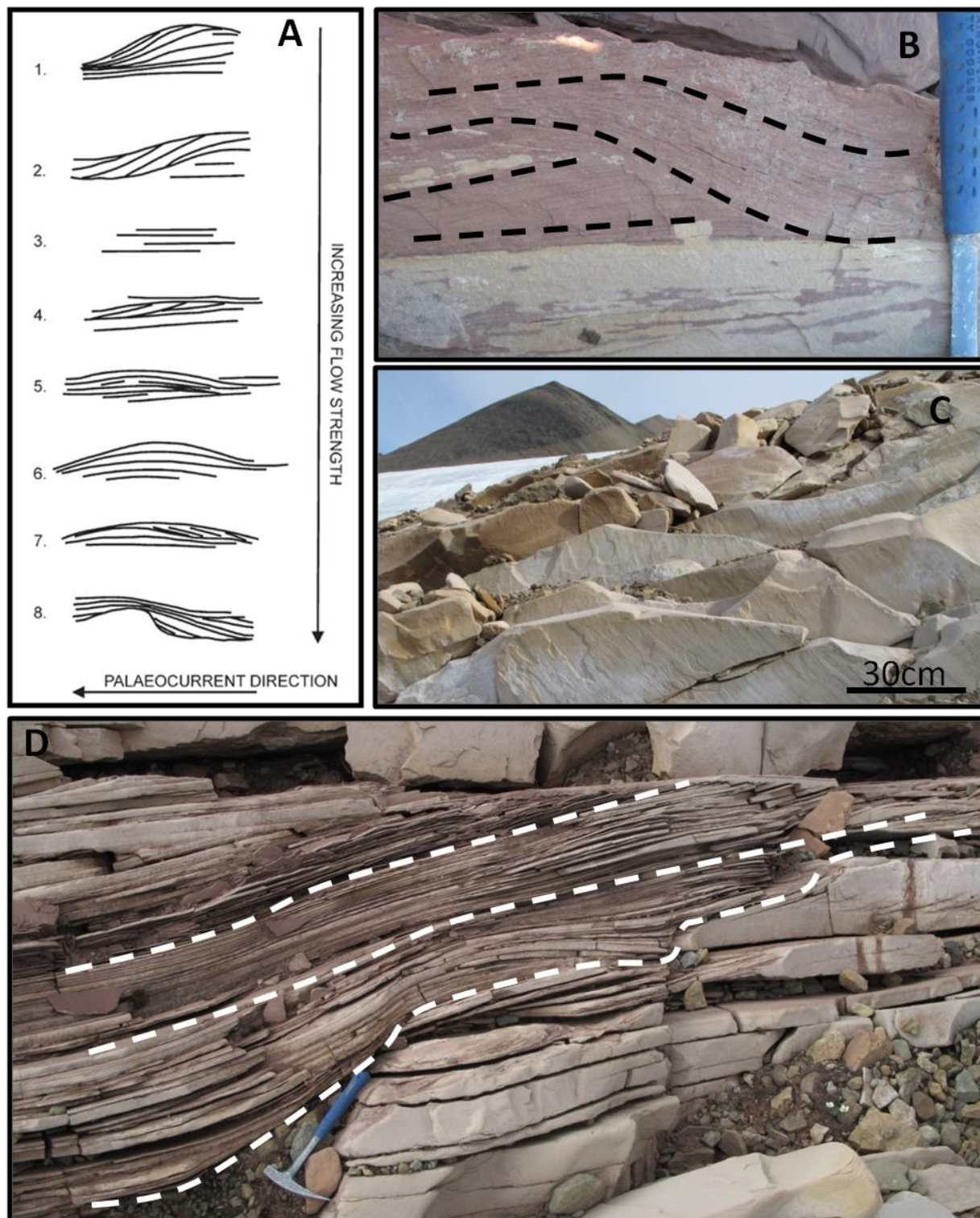
Figure 4.6: Evidence for upper flow regime. A – Interpreted spectrum of sedimentary structures representative of upper flow regime from transitional dunes to chute and pool bedform states (from Fielding, 2006). B – Either transitional dune (2) or transitional antidune (5), lower Cape Butler Mbr; C – Primary current lineation on top of bedding surfaces, present on most of these structures, especially plane bed (3), middle Cape Butler Mbr; D – Possible chute-and-pool structure (8), upper Cape Butler Mbr. Hammer is 30cm long.

arises at a hydraulic jump where shallow, fast-flowing water (the chute) passes abruptly into deeper, less fast-flowing water (the pool). These features are considered to have poor preservation potential which would make the presence of one even more remarkable (Fielding, 2006). Soft-sediment deformation at the base of the Cape Butler Member suggests liquefaction due to rapid sedimentation.

With all the evidence for high flow strength, there is also plenty of evidence for waning flow. The preservation of linguoid ripples is indicative of rapid decrease in flow. Identification of shrinkage cracks (Fig. 4.7A), found entirely in the Cape Butler Member, can be important in interpretation as they can form not only at the sediment-air interface by desiccation processes but also at the sediment-water interface or substratally by synaeresis processes (Plummer and Gostin, 1980). Identification can be difficult as both synaeresis and desiccation cracks can be either non-polygonal or polygonal and have infilling sediment derived from above; however, only synaeresis cracks can have infilling from underlying sediment. Given that there are only three observations of shrinkage cracks, it is challenging to identify the type of shrinkage crack based on the limited data. They all appear with bioturbation, so it is interpreted that they are synaeresis cracks, and are linked to sub-aqueous conditions and surface or substratal dewatering of submerged mud or silt (Plummer and Gostin, 1980).

Well-preserved paleosurfaces (Fig. 4.7B) overlain by the red siltstone deposits host a low diversity, and low to high intensity of trace fossils with a thin siltstone veneer. This requires pulsatory deposition of bedload and suspended-load sediment over short intervals of time (Stear, 1985).

Figure 4.7: Evidence for waning flow. A – Synaeresis cracks in Fl facies from subaerial exposure, middle Cape Butler Mbr; B – Preserved paleosurface on top of multi-storey sand sequence overlain by siltstone, with *Thalassinoides, Skolithos* and a silt veneer, lower Cape Butler Mbr; C – Illustration of Type B climbing ripples from Ashley et al. (1982); D – Type B climbing ripples in Fl facies, with possible draped lamination occurring at top, Cape Butler Mbr; Notebook is 20cm long.

The climbing ripples observed in lithofacies Fl and Sr support aggradation during waning flow. Since the stoss-side of the ripple is preserved, the aggradation rate is greater than the rate of migration of the ripples, which confirms that flow is decreasing and the bedload is falling out of suspension and being deposited rapidly. The climbing ripples grade into possible draped lamination. The ripples climb at angle θ, which is the tangent between the mean migration (V_X) and aggradation rates (V_Y) (Ashley et al., 1982) (Fig. 4.7C). As θ increases, the ripples decrease in steepness and when θ reaches 90°, draped lamination will form. While Type B climbing ripples (Fig. 4.7D) signify relatively high aggradation rates, the rate of migration still exceeds aggradation; in comparison, draped lamination indicates cessation of ripple migration and continued fall-out of suspended sediment (Ashley et al., 1982).

The Bjorne Formation is part of an ephemeral depositional system; while there is a braided fluvial component, there is evidence of sub-aqueous conditions with the presence of trace fossils and synaeresis cracks. The fluvial deposits are made up predominantly of upper flow regime bedforms which are characterized by rapid fluctuation in hydrodynamic conditions with insufficient time during waning flow for the fluvial system to re-equilibrate or rework the bedforms into lower flow regime bedforms; this allows for preservation of these transient features during episodic flow events (Fielding, 2006).

Marine beds are difficult to distinguish from terrestrial beds due to the propensity for trace fossils, for example, the S*kolithos* ichnofacies, can occur in a suite of depositional environments. Fluvial and tidal/subtidal channels are likely comparable, due to suggested low bank stability; with similar sedimentary structures. Given lower bank stability and high and rapid flow power, braided sand sheets are likely to have flowed rapidly into the marine environment allowing the preservation of fluvial, unidirectional flow features in a marine environment.

There is evidence of a mixed marine environment in all three members, but specifically the lower part of the Cape Butler Member due to the relative abundance of trace fossils which potentially represents an increasing marine influence in the distal part of the fluvial system. The presence of herring-bone cross-bedding can be indicative of tidal influence. With the braided river entering a marine influenced system, the channel crosses the threshold into a deltaic environment, however, it does not appear that this changes the channel architecture, so while there could be a rapid transgression depositing mudstone, the overlying sandstones might simply reflect the re-establishment of the fluvial system.

The ancient Campanian Panther Tongue delta in Utah, with sandstone tops bioturbated of the *Skolithos* ichnofacies (Olariu and Bhattacharya, 2006), provides a comparison for bioturbation. Olariu et al. (2005) defined the channels as composed of fine- to medium-grained sandstone, with trough cross-stratified and parallel-laminated bedforms with variable bioturbation intensity and high bioturbation at the top of the beds. Another unit present is parallel laminated sandstone with very fine sandstone to silt with highly bioturbated silty tops. While the channels are characterised as terminal distributary channels, which can be both subaerial and subaqueous in a deltaic environment and have characteristic sedimentary structures of unidirectional flow and show some evidence of reworking by waves and tides (Olariu and Bhattacharya, 2006), the model for bioturbation is similar to the Bjorne Formation. It is possible that the sand sheets of the braided fluvial system extending into the marine environment behaved comparatively to the deltaic channels of the Panther Tongue.

The sandstone bodies in the Bjorne Formation are typically characterized by multi-story, sheet-like beds, particularly evident in the Pell Point Member. Sedimentary structures identified are largely horizontal lamination and lesser low-angle planar and dune cross-bedding, which are

analogous to the deposits of high-energy ephemeral flood events (McKee et al., 1967). The lack

of mudstone in the system, along with the possible decrease in vegetation, could have led to

wide, shallow, unconfined channel systems, promoting the formation of upper flow regime plane

bedding where an ephemeral fluvial braid-plain fed into a deltaic system as a braid-delta

(Eriksson et al., 1995). With the presence of bioturbation and other marine indicators, like

herring-bone cross-bedding, the braided fluvial system would have transitioned into a marine-

influenced environment as sandstone sheets. The architecture of the sandstone units appear

laterally extensive, multistory, and stacked in units a few metres thick, with relatively little

indication of major channel forms. In a more distal environment, the mud content can increase,

which is the case in the lower portion of the Cape Butler Member, and the upper portion of the

Cape O'Brien Member, if covered intervals represent finer sediment. The deposition of silt, and

possibly the covered intervals, suggests the abandonment of braid-delta channels, whether sub-

aqueous or sub-aerial.

The Bjorne Formation represents a system with rapid, ephemeral sedimentation, and given the

proximity to the basin, would have transitioned from a mixed-marine, deltaic environment, to a

non-marine, braided fluvial system. Sediment dynamics within both braided ephemeral and tidal/

subtidal channels of the delta are likely comparable, due to a low proportion of mud and a

possible scarcity of vegetation; channel bank stability could have been limited, promoting the

formation of extensive sandstone sheets (Eriksson et al., 1995). Since lateral continuity of the

lithology and facies was not recorded given the limitation of the section, lateral extent of the

sand sheets are unknown. The ephemeral sand sheets entering the ocean would be deposited,

allowing for a period of quiescence for the occurrence of bioturbation. The depositional regime

of the Bjorne Formation could suggest a paradigm for a braid-delta assemblage, representing

both fluvial and deltaic deposits, influenced by ephemeral sedimentation.

CHAPTER 5: PETROLOGY

5.1 Composition

The thin sections were qualitatively analysed for the mineralogical composition of the sample. Quartz is the predominant mineral in all samples and has no correlation with stratigraphic level in the measured section. Quartz grains range from very fine- to medium-grained with grains in siltstone classified as coarse silt, and grains are very well- to well-sorted. The roundness of grains are largely sub-rounded, regardless of whether the grains display low- or high-sphericity, although determining the sphericity is subject to misinterpretation, as the effects of compaction and cementation can alter the original grain shape. Of the total quartz content (Qt), over 90% is monocrystalline quartz with varying amounts of polycrystalline quartz and chert fragments. Many of the quartz grains demonstrate uniform extinction, but a small proportion display a degree of undulose extinction, a common texture when there is strain in the crystal lattice. There is minimal matrix, but carbonate cement is ubiquitous. The nature of the cement is elaborated in Section 5.3.

Feldspars appeared sparingly in thin section and were identified as microcline and plagioclase. Several feldspar grains were analysed using the microprobe for elemental composition, but only orthoclase ($KAlSi_3O_8$) was identified. In the orthoclase analyzed, Ca, Na, Mg and Fe were present in trace amounts ($< 5\%$), with Ba ~2% in a few grains. Lithic fragments are more common, often about 5% of the bulk composition, and include igneous and metamorphic fragments, metamorphic being more abundant; lithic fragments infrequently appears squeezed. Sedimentary rock fragments are rare, other than chert, in terrigenous sedimentary rocks because they break down fairly easily into their component grains (Adams et al., 1984). Rarely was any lithic fragment or feldspar grain larger than the average quartz grain size. Muscovite is the most

common mica and often appears bent or squeezed between grains. The accessory minerals were sparse throughout the thin sections; however, in order of abundance, zircon, apatite, rutile, tourmaline, monazite and pyrite were observed by optical mineralogy or determined chemically using the electron microprobe. The pyrite is assumed to be diagenetic while the other minerals are detrital. The presence of the detrital grains can be explained by their resistance to chemical weathering and mechanical abrasion, particularly true for zircon, tourmaline and rutile (ZTR), which are considered resistant to weathering and are relatively stable, dense minerals in surficial settings. As a result of higher specific gravities, heavy-mineral grains tend to be smaller than quartz (Tucker, 1991), and that is observed in the Bjorne Formation.

There is a high proportion of quartz, chert and ultrastable heavy minerals indicating a mineralogically mature suite of sediment. The majority of samples contain minimal clay, are well-sorted and sub-rounded, representative of a mature stage of textural maturity. Through qualitative analysis, the Bjorne Formation samples display both mineralogical and textural maturity.

From the data collected, two ternary plots were generated, one from McBride (1963) and the other from Folk (1974). Samples on the Folk plot (Fig. 5.1A) are distributed between quartzarenite and sublitharenite. Samples on the McBride plot (Fig. 5.1B) are distributed primarily in the quartzarenite field. The classification of quartzarenite is congruent with the interpretation of mature sediment, as quartzarenite is always mineralogically mature.

5.2 Provenance

The detrital composition of sandstone is strongly influenced by the tectonic setting of its provenance region as plate tectonics controls the distribution of different types of sandstone. Dickinson and Suczek (1979) showed that the mineralogical composition of sandstone derived
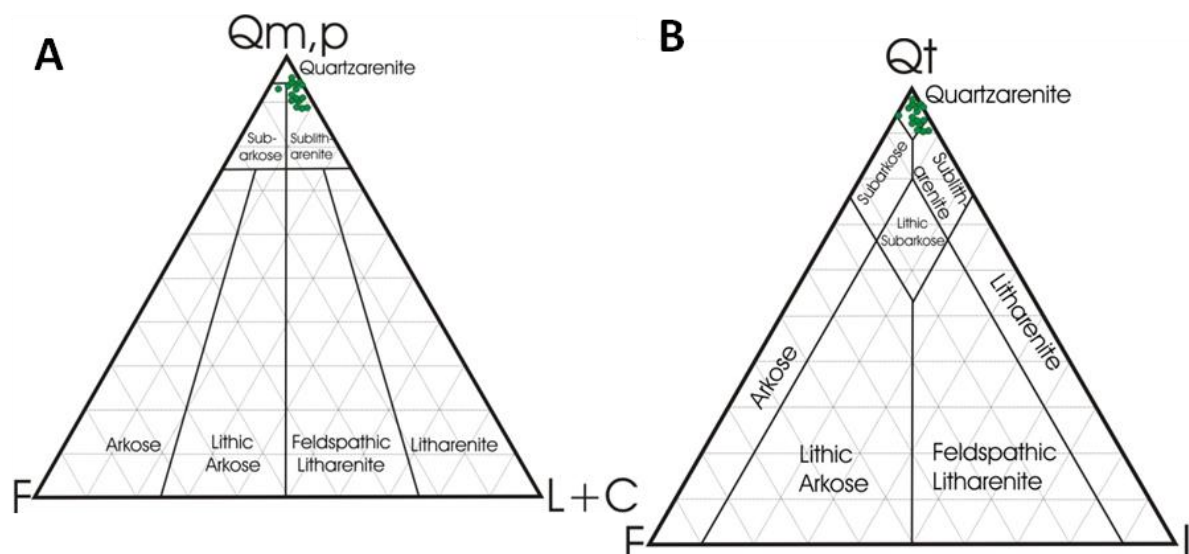
Figure 5.1: Sandstone classification ternary diagrams, A – Folk classification (1974); B – McBride classification (1963); Qm,p – Mono and polycrystalline quartz, Qt- all quartz including chert, F – Feldspar, L – Lithic fragments, L+C – Lithic fragments including chert.

from specific provenance terranes controlled by plate tectonics lies within distinct fields when plotted on ternary diagrams. The modal concentrations are volumetric proportions of the following categories (Dickinson et al., 1983):

A: For QtFL diagrams, the poles are (1) total quartzose grains (Qt) including polycrystalline quartz and chert; (2) feldspar grains (F); and (3) unstable polycrystalline lithic fragments (L) of either igneous or metamorphic variety.

B: For QmFLt diagrams, the poles are (1) monocrystalline quartz grains (Qm); (2) feldspar grains (F); and (3) total polycrystalline lithic fragments (Lt) including polycrystalline quartz fragments.

By plotting all quartzose grains together, the QtFL diagram emphasizes grain stability, and thus focuses on weathering, provenance relief, and transport mechanism. In contrast by plotting all lithic fragments together, the QmFLt diagram emphasizes the grain size of the source rock, because finer grained rocks yield more lithic fragments in the sand-size range (Dickinson and

Suczek, 1979). When plotted, the QtFL diagram (Fig. 5.2A) suggests a provenance setting of recycled orogen, and to a less extent, craton interior. The QmFLt diagram (Fig. 5.2B) is similar, but predominantly suggests a craton interior setting rather than quartzose recycled (recycled orogen).

The source of sediment into the Sverdrup Basin is largely from the south and east, over the Canadian and Greenland Shields (Patchett et al., 2004). There was minor input from a northern source, Crockerland; however, it contributed an insignificant amount of sediment during its time as an active source from the Carboniferous to Jurassic. The cratonic interior is intuitive with the large Precambrian Canadian and Greenland Shields lying to the south and east respectively. The provenance setting of recycled orogen may fit with sources from the shields which consist of former orogenic belts. The work by Patchett et al. (2004) and Miller et al. (2006) has enabled the Dickinson provenance plots to be better comprehended.
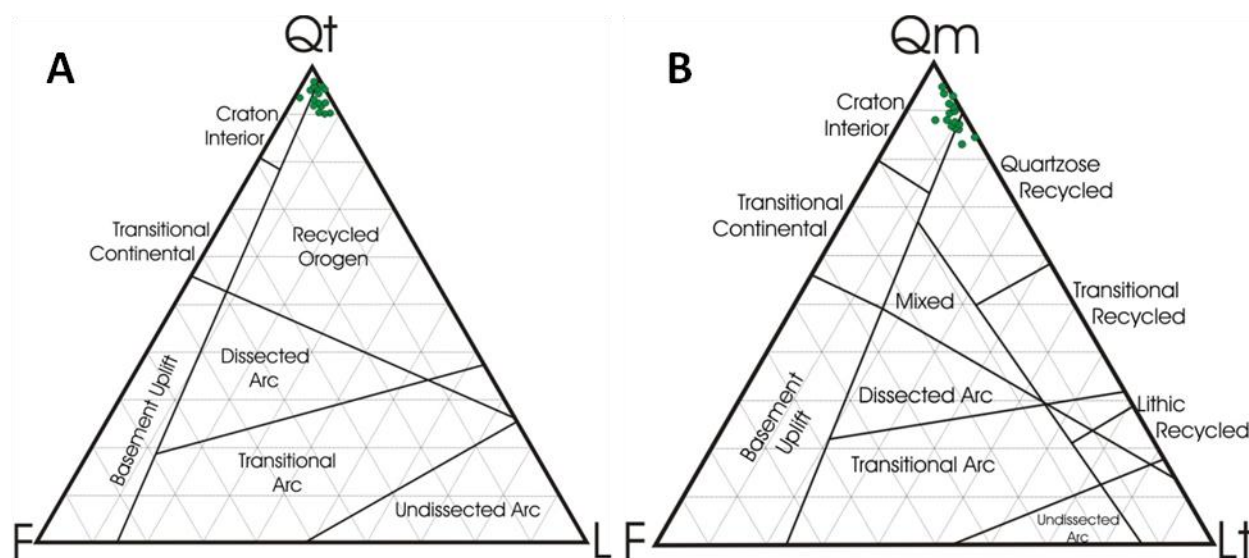
Figure 5.2: Triangular QtFL (A) and QmFLt (B) plots for framework modes of terrigenous sandstones showing subdivisions according to inferred provenance types determined by Dickinson and Suczek (1979)

Patchett et al. (2004) used Sm-Nd isotopic analysis coupled with trace element characterization, and demonstrated that, for most of Carboniferous to Late Cretaceous time, the sediment supply in the Sverdrup Basin was from a single broad provenance with sediment from Caledonian/Ellesmerian mountains dominating the provenance of the continental and continent-margin sedimentary system for at least 370 Myr., a period extending far beyond the existence of the mountains themselves. The sediment from these orogenic events collected in a foreland basin and further over the craton and is termed the Devonian Clastic Wedge. Figure 5.3A illustrates the source of the Devonian siliciclastics in the northeastern Canadian Arctic region. Middle-Upper Devonian clastic strata are up to 4,000 m thick and were deposited in a foreland basin which developed south and east of the Ellesmerian Orogenic Belt (Embry, 1988).The Devonian sediment was subsequently recycled and was the supply source during the Early Triassic which marks the beginning of a major progressive removal of the wedge which continued throughout the Mesozoic. The tectonic history during the period in the Arctic region is summarized in Figure 5.3B.

Miller et al. (2006) sampled detrital zircons from Triassic sandstones from the circum-Arctic region, dated by laser ablation-inductively coupled plasma-mass spectrometry. One of the sites samples the Smithian, braided-stream facies of the Bjorne Formation from central Ellesmere Island (Fig. 5.3C). As a consequence of plate collision between the eastern margin of Baltica and eastern Laurentia in the Silurian (445–420 Ma), the Caledonian mountain formed (Harrison, 2005). The peak age of the zircons at the site is 454 Ma, which is representative of zircons from older rocks deformed in the Caledonian Orogen. There are zircons dated from about 350 Ma, which coincide with the Ellesmerian Orogeny and initial rifting of the Sverdrup Basin. The Late
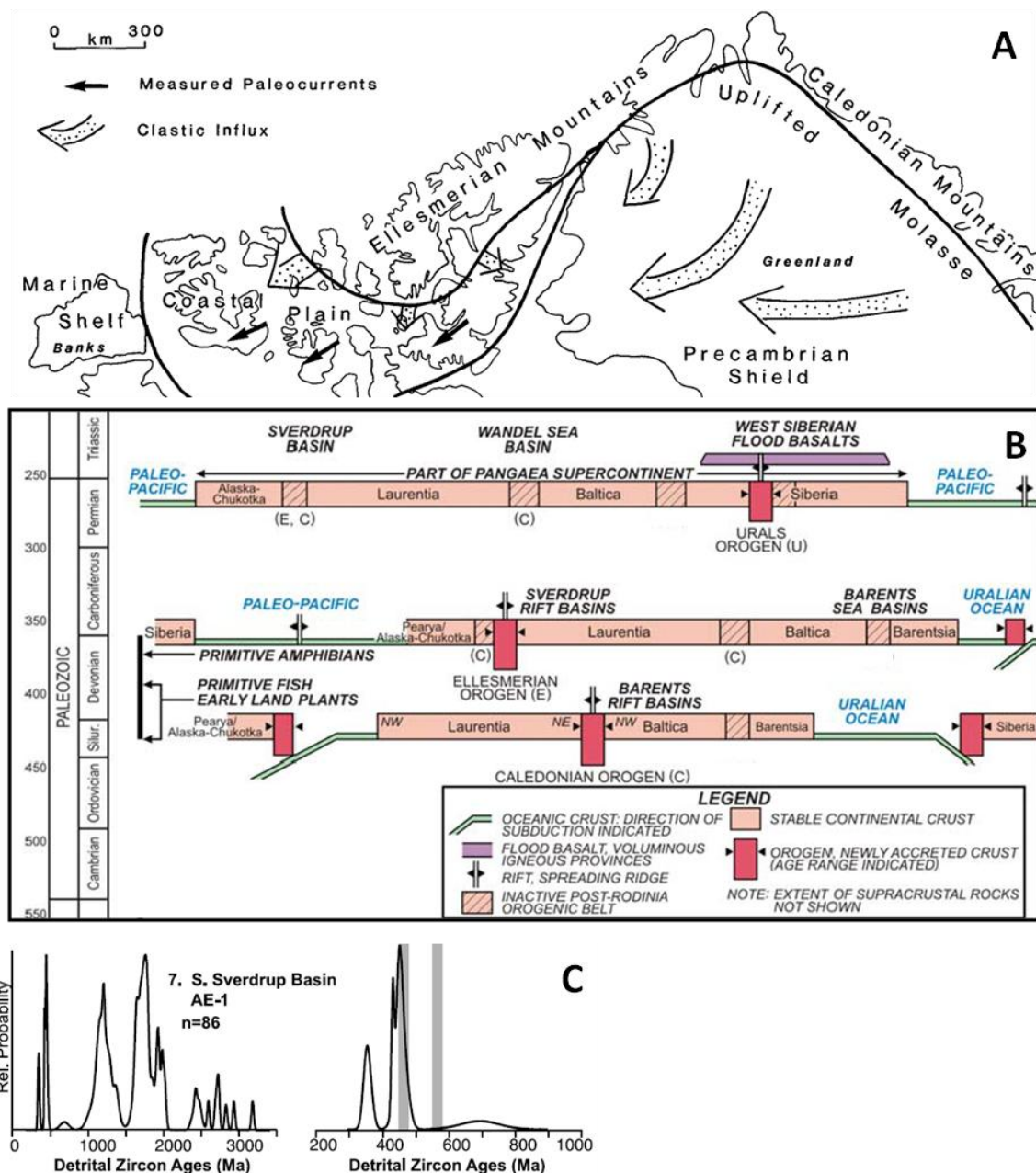
Figure 5.3: A – Late Frasnian Paleogeography (~380 Ma); B – Schematic cross-sections highlighting tectonic events in the Arctic region; C – Relative probability distribution diagrams for detrital zircon U-Pb ages from Bjorne Fm, On the left, spectra include all of the ages from each sample. On the right, spectra include only ages <1000 Ma (from Embry, 1988; Harrison, 2005; Miller et al., 2006, respectively).

Devonian-Early Carboniferous Ellesmerian Orogen was produced by the tectonic accretion to

northern Laurentia of lower Paleozoic volcanic arcs and displaced continental fragments such as

Pearya and Arctic Alaska-Chukotka (Harrison, 2005). The rest of the zircons from the Bjorne

Formation yield Precambrian ages with probability peaks evident at 1216, 1662, 1769, 1933, and

1988 Ma. These grains clearly are from the Canadian, Greenland Shield or possible even further, from the Baltic Shield, but an issue is that the Canadian and Greenland Shields were covered with sediment of the Devonian Clastic Wedge, so the Precambrian ages from Lower Triassic zircons are not directly sourced from the shield. The sediment in the Devonian Clastic Wedge is in part from recycled sands from the Precambrian shield as well as the Caledonian and Ellesmerian orogenies which explains the highly quartzose nature of the Bjorne Formation. Ternary plots and previous data confirm the recycled orogen and craton interior provenance for the Bjorne Formation. Given the recycled nature of the sand, the provenance signature was inevitable, but the original sands may have formed in a very different tectonic setting.

5.3 Diagenesis

Pure quartz sandstone presents the smallest opportunity for diagenetic alteration, so the proportion of the sandstone which is not quartz is significant (North, 1985). Carbonate is one of the most common cements in sandstone, and that is no different in the Bjorne Formation where carbonate cement is prevalent in variable amounts throughout the formation. This is not anomalous or unusual as carbonate cements are especially characteristic of fine-grained sandstone with excellent initial sorting and high total cement contents (North, 1985). The diagenetic cement ranges from 15 to 45% of the bulk rock volume.

The degree of carbonate cementation appears to have no relationship with stratigraphic level. Types of carbonate cement include poikilitic, euhedral rhombohedra, fine-grained aggregates and infilling of micro-fractures. In many of the thin sections, the grains have a floating contact as a result of carbonate cementation displacing grains, or filling spaces between loosely compacted sediment. The zoned rhombohedra (Fig. 5.4A) are dolomitic and many have a hematite rim. The electron microprobe was utilized to find the composition of the dolomite. The well-formed,
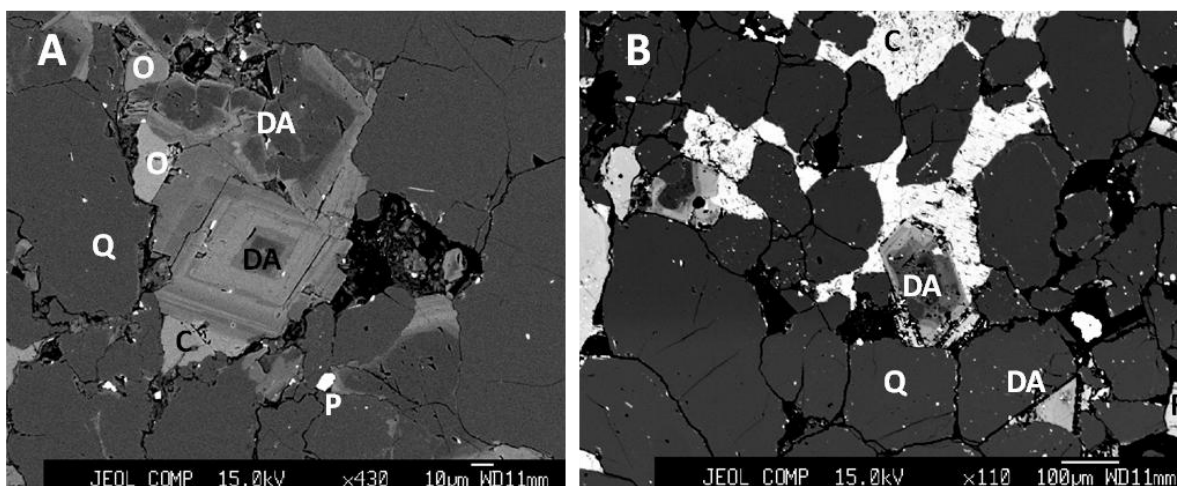
Figure 5.4: Images from electron microprobe. A – Zoned dolomite -ankerite rhombohedra, slide DM-09; B – Dolomite-ankerite replacing calcite cement, DM-15; C – Calcite, DA – Dolomite-Ankerite, O – Orthoclase, P – Pyrite, Q – Quartz.

microcrystalline rhombs are the only form of dolomite cement present and are increasingly ferroan towards the rim. Iron-rich dolomite is indicative of precipitation in reducing conditions and magnesium for later dolomite precipitation may be derived from clays or dissolution of magnesium-rich silicates (Tucker, 1991). Typically, with the increase in iron, magnesium decreases with minimal substitution of calcium cations; therefore, the rhombohedra form a solid solution series between dolomite and ankerite which is clear in Figure 5.5 as the dolomite becomes increasingly ferroan. The rhombs have a cloudy core, possibly due to calcite relics, and become progressively clearer towards the rim (Fig. 5.4). Many of the rhombohedra have surrounding calcite with hematite present as a very thin coating around grains. Hematite cement is also present as grain coating for quartz, but it is predominantly around carbonate grains. The carbonates in the Bjorne Formation are interpreted as pore-filling calcite, and grain-replacive and pore-filling dolomite-ankerite.

It can be interpreted that the Bjorne sandstones underwent early cementation by calcite occurring at relatively modest temperature conditions from bicarbonate-rich groundwater whereas dolomite-ankerite formed under more advanced diagenetic conditions. Deep-basin
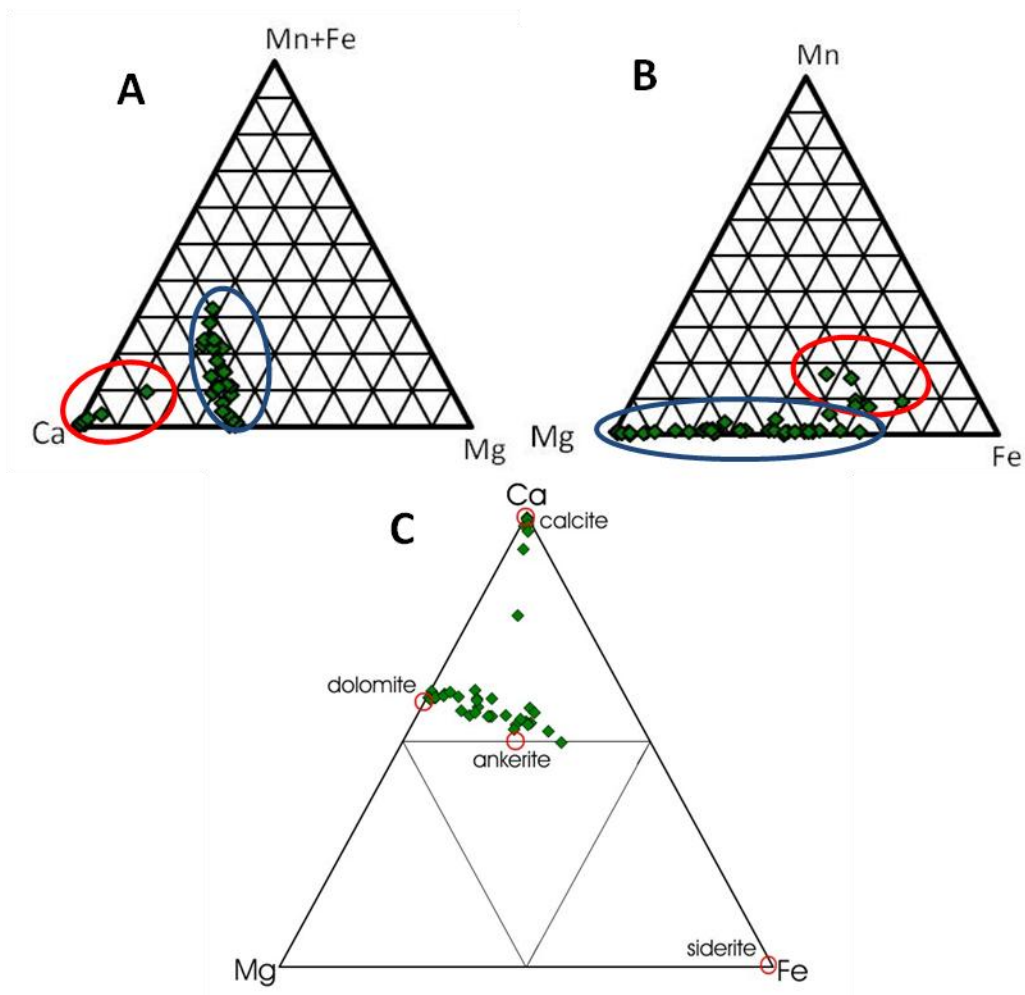
Figure 5.5: A,B – Ternary plots showing major and trace element compositions of early and late carbonate cement, red circle – Calcite, Blue circle – Dolomite-ankerite; C – Chemical composition of diagenetic carbonates based in chemical analyses on Deer et al. (1970). Data determined by electron microprobe, see appendix for full chemical analysis.

diagenesis liberates Fe and Mg from clays and rock fragments, which becomes available for

rhombohedra to develop. When Mn is slightly enriched in the early phase calcite, it can indicate

the source of the water. Fresh waters have greater than 96 mol% Ca, are Mn-rich relative to

calcite from marine waters, and have lower Fe and Mg content than evolved marine fluids

(Hayes and Boles, 1993). According to the triangular plot in Figure 5.5, the early calcite cement

has very high mol% of Ca and is enriched in Mn, as well as Fe, than compared to Mg. While

diagenetic fluids are complex, this could suggest that the calcite cement formed in pore space by

direct precipitation of a mixture between fresh and marine pore waters, similar to what was recorded by Kim et al. (2007) in part of the Tetori Group of Japan.

Albitization of feldspar is a common occurrence during diagenesis; however, it is difficult to observe using optical textures. Cathodoluminescence or further microprobe work is needed to determine the level of albitization by analyzing the Na-Ca ratio in the minimal plagioclase (Fig. 5.6F) found in thin section, although most sandstones extensively cemented by calcite during early diagenesis exhibit weak to no plagioclase albitization (Kim et al., 2007).

Silica cementation occurs as rare quartz overgrowths, but occurs significantly less than the carbonate cement, with the quartz overgrowths appearing volumetrically minor. There is a possibility that some of the recycled quartz grains had overgrowth remnants still visible. A proportion of detrital quartz is not the only requirement for the development in quartz cementation, but is more related to depositional environments as quartz cement is uncommon and volumetrically negligible in delta plain deposits (Kim et al., 2007). The early precipitation of carbonate inhibits later quartz overgrowth formation and feldspar alteration to clays (Tucker, 1991). In view of the rarity of quartz overgrowths, it was difficult to constrain the relationship between early carbonate cementation and silica cementation.

Quartz grains have long and point contacts, but often when carbonate cement is widespread, the contacts between grains are floating (Fig. 5.6E). The grains are rarely sutured (Fig. 5.6A), but some have undergone solution leading to the penetration of one quartz grain into another, which is referred to as concavo-convex contacts (Fig. 5.6E). This is the first stage of pressure-solution; contacts are sutured when pressure-solution is more intense (Adams et al., 1984). Pressure solution is less intense at grain contacts when the sediment is cemented early, before deep burial
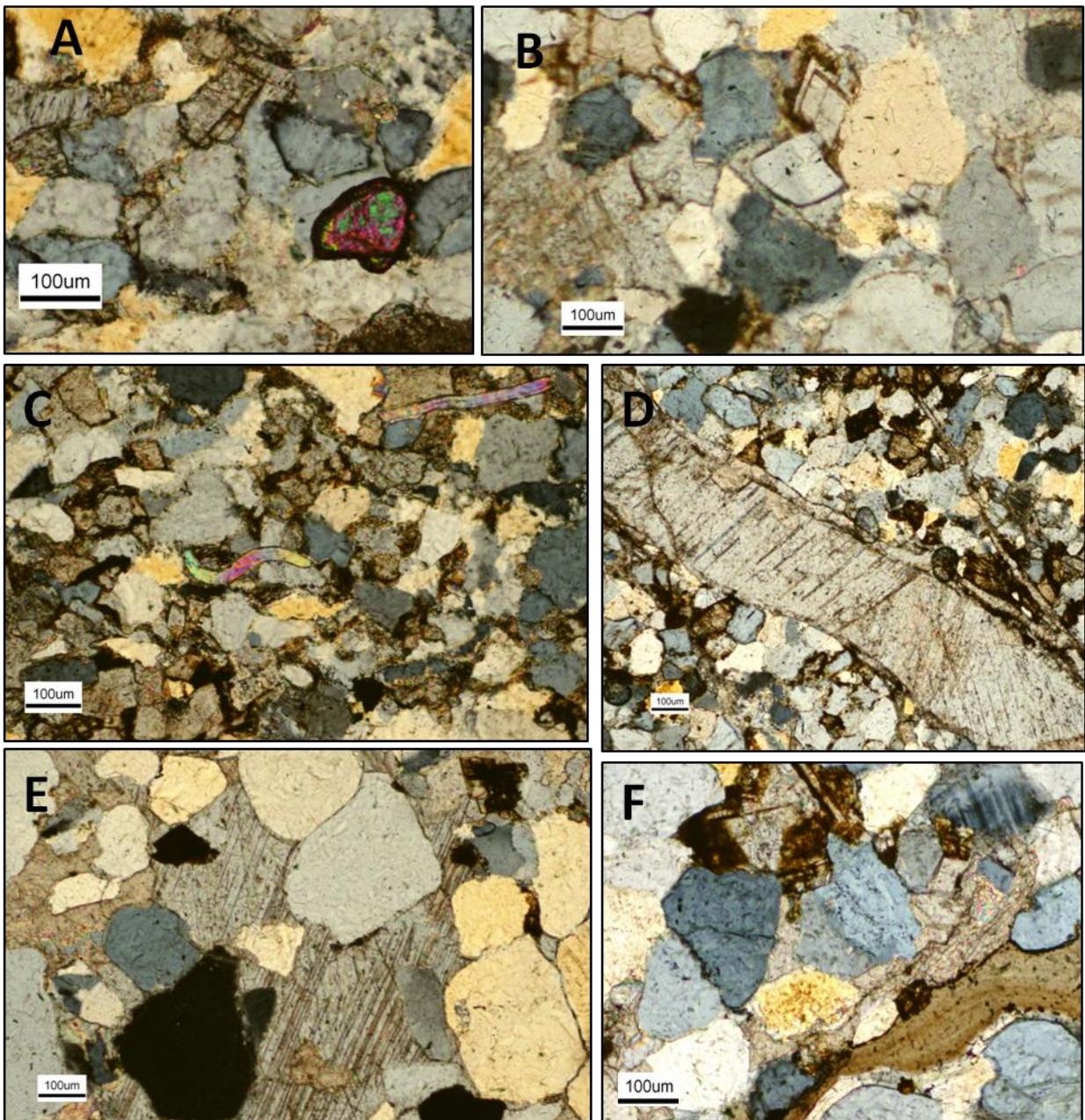
Figure 5.6: Images from microscope; A – Zircon grain, sutured contact (arrow), lithic grain at bottom right, Slide DM-07; B – Dolomite-ankerite rhomb with hematite grain coating, Slide DM-03; C – Bent muscovite, dolomite-ankerite rhombs, Slide DM-09; D – Calcite infilling microfracture, Slide DM-11; E – Poikilitic calcite, quartz grains exhibiting a variety of contacts including floating, slide DM-14; F –Plagioclase, slide DM-15.

because the load is spread and the contact pressure reduced (Tucker, 1991). Pressure solution was more commonly observed in samples in the lowermost member, with sutured contacts more prevalent than compared to the Pell Point and Cape O'Brien members.

Compaction relates to textural and mineralogical maturity, and since the Bjorne Formation is primarily quartzarenite, it undergoes less loss of porosity than a feldspathic sandstone because feldspars partially or completely decompose to form clay (North, 1985). Further compaction is evident by the presence of squeezed mica grains (Fig. 5.6C) and lithic fragments with the latter possibly been compacted from previous burial. Lithic fragments tend to be readily deformed or crushed by overburden, and would accelerate the reduction of porosity by simple compaction as the depth of burial increases (Dickinson and Suczek, 1979).

Early stages of burial include pore-filling calcite and mechanical compaction. The grain boundaries of quartz do not imply significant compaction which is further evidence of early
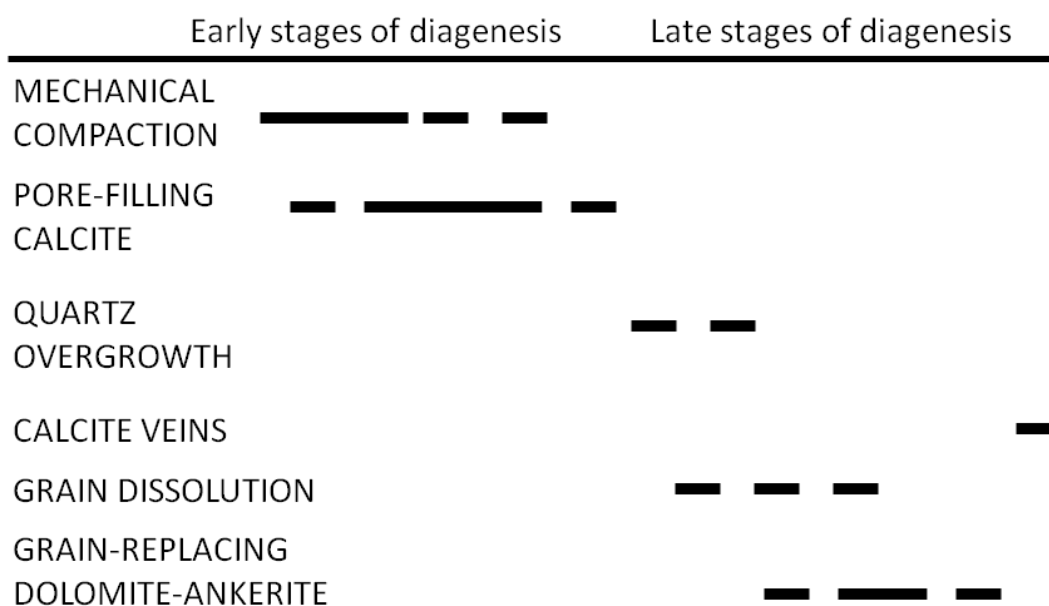
Figure 5.7: Diagenetic evolution of Bjorne Formation

cementation during diagenesis. The lack of quartz overgrowths also implies early cementation of carbonate. Later stages of burial include minor quartz overgrowth, and grain-replacive and secondary pore-filling dolomite-ankerite rhombohedra, solely replacing the earlier pore-filling calcite cement. Calcite vein fills are assumed to have occurred later in diagenesis, possibly during uplift as no rhombohedra occur in the veins. Figure 5.7 illustrates the interpreted diagenetic evolution of the Bjorne Formation.

Poursoltani and Gibling (2011) summarized the range of temperatures needed for specific diagenetic features to occur from a variety of papers regarding burial in the Gulf Coast. In the Gulf Coast Basin, pore-filling calcite cements occur in the 20-70°C range, quartz overgrowths precipitate at 55°C or higher, dissolution of feldspar can occur from 90-160°C, and ankerite, as late-stage replacement of calcite has a temperature range of 80-145°C. These values are generalizations of temperatures the Bjorne sandstone could have encountered during diagenesis, and are based on estimates from a single basin. Further work is needed to constrain burial temperatures.

Figure 5.8: Porosity vs. Depth, summary of 120 data points from Arctic wells intersecting the Bjorne Formation and displaying average and maximum values at intervals of 900, 1100, 1700, 2000, 2200, 2700, and 3000 m.

5.4 Porosity

Porosity is controlled by grain size, sorting and shape, method of deposition and effects of compaction. The sands of

the Bjorne Formation are fine-grained, which encourages lower porosity values than coarser-grained sand, but are well-sorted from deposition, thus being more porous than poorly sorted sediment. With the help of Keith Dewing at the GSC, a compilation of individual porosity data points from wells are plotted against depth below surface (Fig. 5.8). The diagram illustrates the decrease in porosity with depth, but displays, on average, good porosity up to 2,000 m depth. The depth intervals have average porosity values ranging from ~5% to ~20%, and have several intervals with maximum porosity ~25%. The sands present in the Bjorne Formation are interpreted to have been deposited under high-energy conditions, and the original porosity in high-energy sands is typically 40-55%, and the permeability 25-100 D (North, 1985). The effects of cementation and compaction during diagenesis clearly reduce porosity and permeability values. Core grain density is important in core analysis as it is a quality control check and is used in the equation to calculate porosity. Sandstone has an approximate grain density of 2,650 kg/m^3; therefore, the distribution in Figure 5.9 is expected for a predominantly sandstone unit, like the Bjorne Formation.

Analysis of porosity and permeability in the Bjorne Formation has been summarized in Figure 5.9 by Hu and Dewing (2010). The permeability ranges from <0.01 mD to >1000 mD. Three thin sections stained with blue epoxy (Fig. 5.10), one from each member of the Bjorne Formation (Table 5.1). The porosity appears to be principally secondary, which correlates to early calcite cement filling in initial pore space. It is from dissolution of grains that creates the secondary porosity, as wells as possible fracturing (Slide DM-15, Fig. 5.10). The ferroan-dolomite/ankerite is suggested to postdate the main phase of calcite cementation and generation of secondary porosity, which is in accordance with other studies with late phase development during
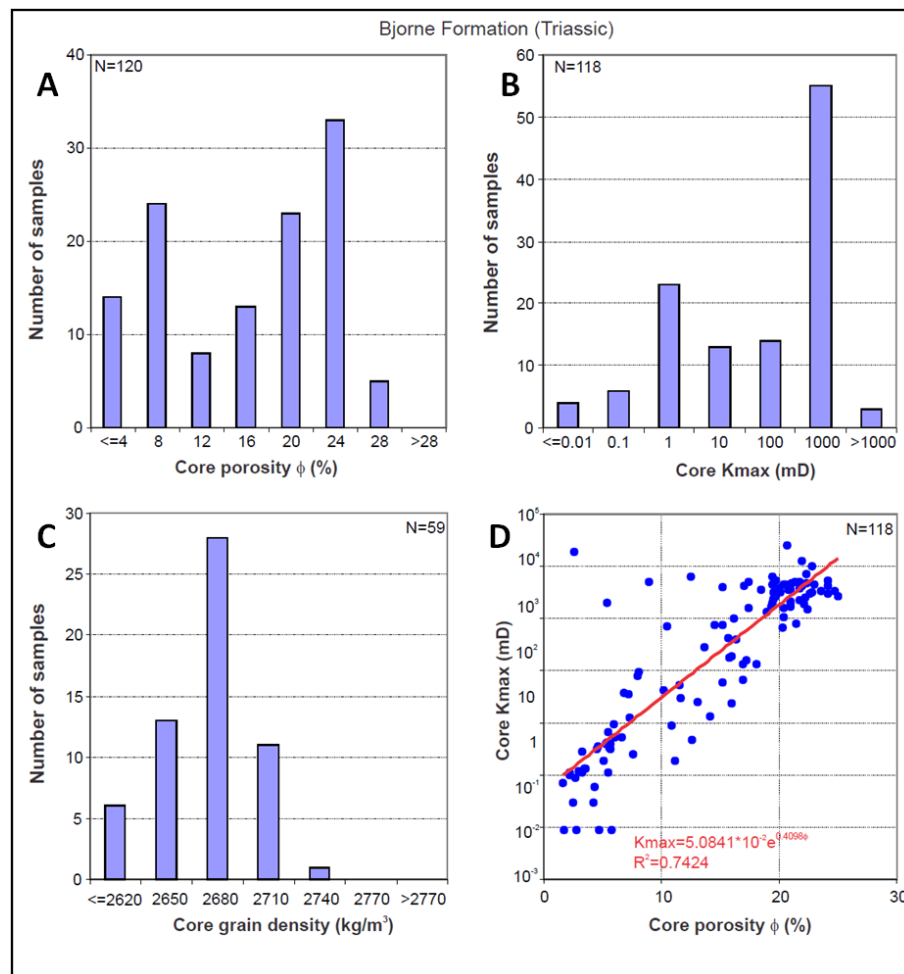
Figure 5.9: A – Distributions of core porosity; B – permeability; C – grain density; D – core porosity-permeability cross plot for the samples from Bjorne Formation; N – number of samples (from Hu and Dewing, 2010).
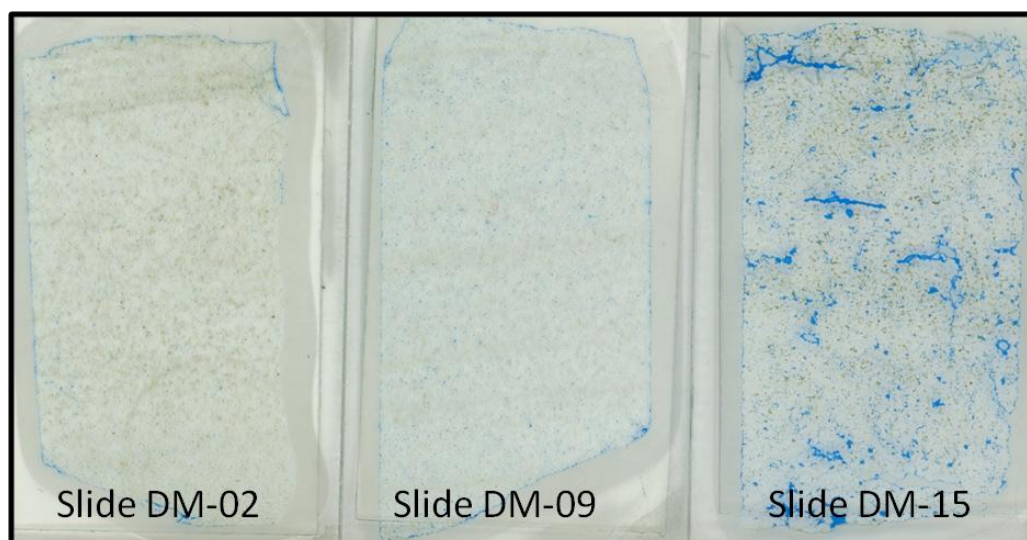
Figure 5.10: Three slides stained with blue epoxy, used for point counting method; slides are 4.5 cm long and 2.5 cm wide.

Slide	Void Space Count	Grain Count	Total Counts	Porosity
DM-02	17	282	299	6%
DM-09	24	300	324	7%
DM-15	61	267	328	19%

Table 5.1: Porosity values from point count method.

Porosity (%)	Qualitative Evaluation	Permeability (mD)	Qualitative Evaluation
0 - 5	Negligible	< 1.0 - 15	Poor to fair
5 - 10	Poor	15 - 50	Moderate
10 -15	Fair	50 - 250	Good
15 -20	Good	250 - 1000	Very good
20+	Very good	>1000	Excellent

Table 5.2: North's (1985) qualitative evaluation of porosity and permeability.

diagenesis (Kim et al., 2007; Poursoltani and Gibling, 2011). The calcite cement occluded primary porosity, but grain dissolution created secondary porosity. The subsequent grain-replacive dolomite-ankerite would therefore have filled in the secondary porosity; however, later veining and fracturing could provide adequate porosity. Slide DM-15 has outsized pores, larger than the average grain size as well as large open pores; it is possible that this is a trait from the hand sample, or that more fracturing has occurred in the uppermost member. The rhombohedra are larger in slide DM-15 compared to DM-09, possibly because there was more secondary pore space to grow into. Slide DM-09, and -02 have very poor interconnectivity of pores, likely yielding lower permeability values than slide DM-15.

The porosity values from thin section have a lower average than the GSC data; however, the Cape O'Brien Member has higher porosity than the core analysis average. Whether the sample from the Cape O'Brien Member is anomalous or representative of a different burial history than the lower two members is unknown. According to North's (1985) qualitative evaluation of

porosity and permeability (Table 5.2), the Bjorne Formation has very good to poor porosity using either data from point count or core analysis and generally very good permeability from core analysis.

5.5 Thermal Maturity

Time and temperature are vital factors for the formation of petroleum. Vitrinite reflectance (R_o) is used to provide a maturity index because it is temperature and time dependent. It needs no correction for uplift, or erosion as it is an irreversible technique, making it a useful method for determining the likelihood of hydrocarbon generation (North, 1985). Waples (1980) defined the important stages for hydrocarbon generation: onset of oil generation (R_o = 0.5%), peak oil generation (R_o = 1.0%), end of oil generation (R_o = 1.30%), upper limit for occurrence of wet gas (R_o = 2.2%), and last known occurrence of dry gas (R_o = 4.8%).

In Figure 5.11, the data is from the most proximal well to the study area, Fosheim N-27 (location of well shown in Figure 1.2), drilled in the centre of the depocentre where Lower Triassic strata approaches 2,400 m in thickness including igneous intrusions, but a thrust fault repeats a substantial part of the Bjorne Formation. Vitrinite reflectance from the top of the Bjorne Formation and the overlying Murray Harbour Formation has values of about 0.8 to 1.3%, with samples in the oil window, and close to peak oil conditions. The Blind Fiord Formation and Permian strata are in the gas window with values ranging between 1.5 and 3.3%.
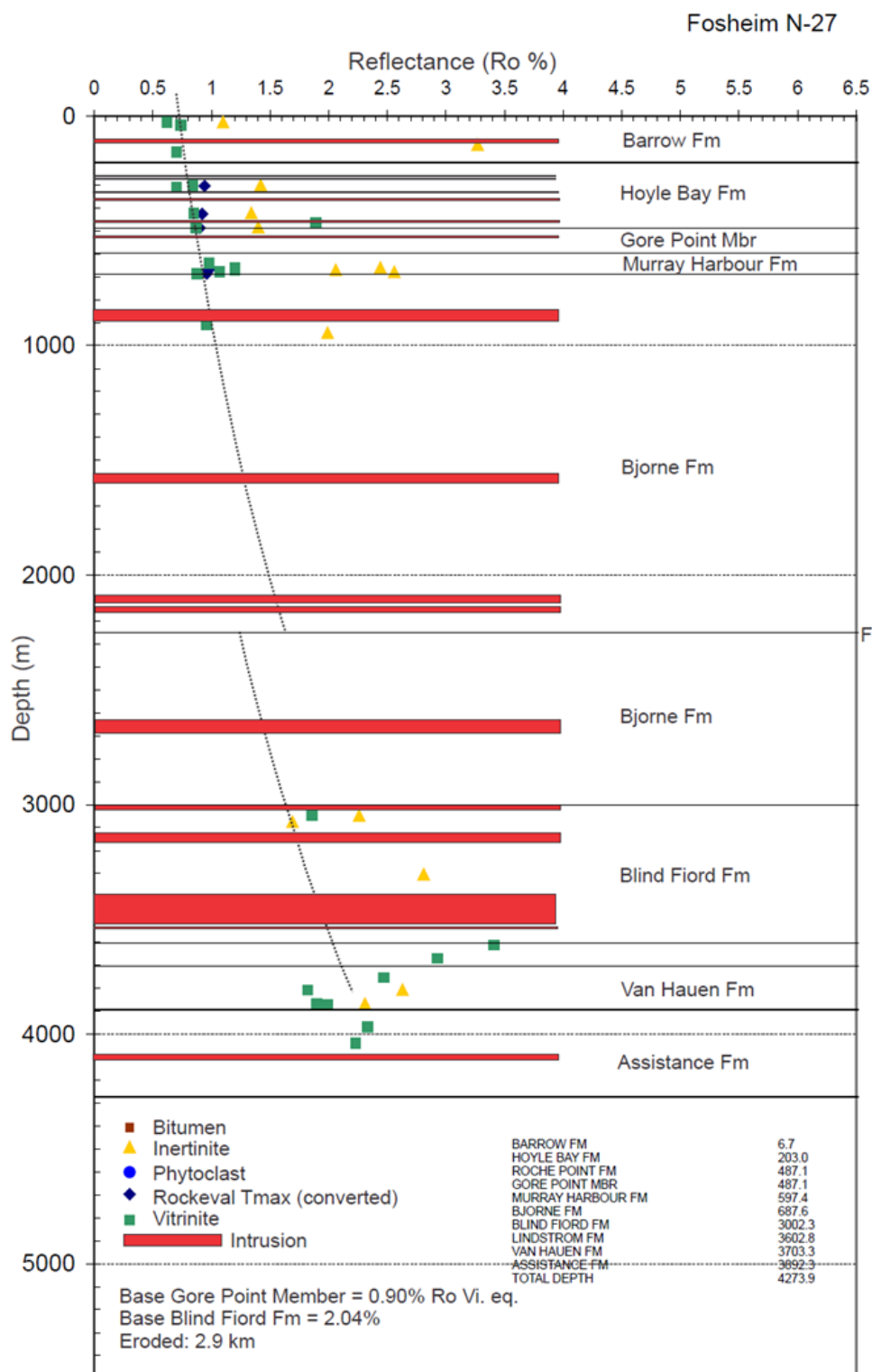
Figure 5.11: Thermal maturity taken from Fosheim N-27 well, drilled on the Fosheim Peninsula; F – fault.

CHAPTER 6: DISCUSSION

6.1 Permian-Triassic Extinction

The Permian-Triassic boundary event represents the largest extinction event in the geological record, during which 80-97% of all species died out (Retallack, 1995). The timing of the event is subject to some debate. In the Sverdrup Basin, the extinction event is placed in the latest Permian, which is placed at the basal Blind Fiord Formation contact. The base of the Triassic is located 31.75 m above the base of the Blind Fiord Formation in northwest Ellesmere Island, which indicates that the extinction event occurred during the Late Permian, before the onset of Triassic sedimentation (Beauchamp et al., 2009). Deposition of the Bjorne and Blind Fiord formations began in the earliest Triassic, so the extinction event could have had a pronounced effect on the sedimentation.

Vegetation has a marked impact on fluvial systems by altering the mechanisms of flow and deposition. With a limited amount of terrestrial vegetation, the tendency would increase for flashy surface runoff, lower bank stability and faster rates of channel migration. For this reason, bedload-dominated, sheet-like, braided alluvial deposits dominated in the Precambrian and early Paleozoic (Long, 2011). Surface run-off is more rapid in the absence of rooted vegetation, causing fluvial systems to be dominated by upper-flow regime conditions due to more pronounced peaks in precipitation and run-off. With roots absent, erosion is significantly greater as modern sand bars would lack stabilization, and bare surfaces are up to 20,000 times less stable than sand with 16-18% roots (Smith, 1976). Upstream areas would not have the capacity to hold excess water, so downstream parts of the catchment area would be subject to ephemeral, intense discharge with periods of rapid drying out (Gouramanis et al., 2003). Davies and Gibling (2010) reviewed the evolution of fluvial styles, and before the onset of vegetation in the Silurian-

Devonian, rivers were predominantly braided with extremely rare occurrences of meandering or anastomosing deposits. If the lack of vegetation had a significant effect before the evolution of terrestrial plants, it is highly probable that after the widespread extinction of rooted plants during the Permian-Triassic event, sedimentation systems would have been altered.

Around the world, changes in sedimentation rate and style have been observed across the Permian-Triassic boundary. The cause of the latest Permian mass extinction is subject to some debate, but the leading hypothesis is that the extinction was a globally synchronous event triggered by the (main-stage) eruptions of the Siberian Traps volcanic province, the largest eruption of flood basalts during the Phanerozoic, the age of which is indistinguishable from that of the ca. 252 Ma Permian-Triassic boundary (Algeo et al., 2012). Eruptions occurred before the main-stage and are thought to have begun during the early Late Changhsingian (Grasby et al., 2011), up to several hundred thousand years prior to the latest Permian mass extinction and thus roughly contemporaneous with marine environmental changes in the Sverdrup Basin and with changes in intermediate-depth marine systems globally, as reported by Algeo et al. (2012). Figure 6.1 outlines the global timeline of events, compared to the Sverdrup Basin, from the Late Permian to Early Triassic.

The Siberian Traps released a substantial volume of volcanic CO_2 and methane into the atmosphere, triggering strong climatic warming, as shown by oxygen isotopic studies (Kearsey et al., 2009). The volcanic emissions are likely to have increased the acidity of precipitation (Wignall, 2007), which, along with climatic warming, resulted in elevated rates of chemical weathering (Retallack, 1999). These changes would have been important factors in the latest Permian destruction of terrestrial ecosystems which did not recovery rapidly after the event.
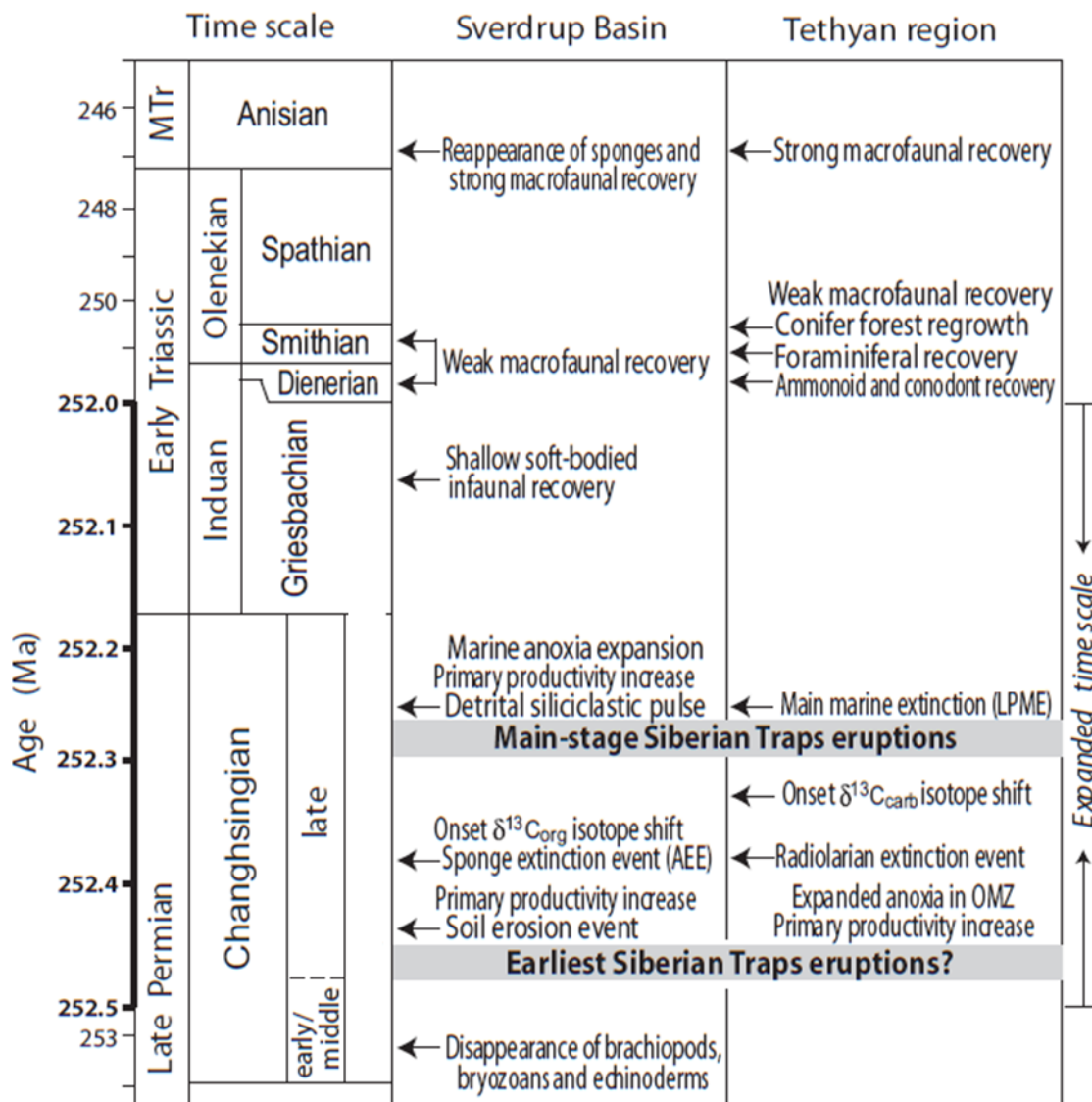
Figure 6.1: Time line of events in the Sverdrup Basin and Tethyan region during the Late Permian and Early Triassic. Late Changhsingian extinctions of sponges in the Sverdrup Basin and radiolarians in the Tethyan region predate main-stage Siberian Traps eruptions by ~100 k.y. Note location of AEE vs. LMPE, MP—Middle Permian, MTr—Middle Triassic; LPME— latest Permian mass extinction; AEE—Arctic extinction event; OMZ—oxygen minimum zone (from Algeo et al., 2012).

Accelerated erosion rates followed with the decimation of forests in the latest Permian, and reduced erosion coincided with the regrowth of forests in the late Olenekian (Looy et al., 1999).

Algeo et al. (2012) proposed that an increased flux of detrital siliciclastics to the Sverdrup Basin commenced in the early part of the late Changhsingian. This event was ~0.1 Ma prior to the onset of increased sediment flux in the Tethyan region in the latest Changhsingian caused by

the Latest Permian Extinction. This earlier event is named the Arctic Extinction Event and corresponds with the early stages of the Siberian Traps. More northerly sites may have been more vulnerable to deposition of acidic gases and ash from early stages of the Siberian Traps eruptions (Grasby et al, 2011), and in the latest Permian, the Sverdrup Basin was located at ~40°N (Fig. 6.2), which was much closer to the Siberian Traps volcanic centers at 60–70°N in terms of both paleolatitude and absolute distance (~3,000–4,000 km) than were sites in the Tethyan region (Algeo et al., 2012). The earlier Arctic Extinction Event could have resulted in elevated subaerial weathering rates in the region compared to regions further from the initial out-gassing from the volcanic eruption; subsequently, global systems would have been altered by the main-stage eruption of the Siberian Traps.

A basin-wide die-off of terrestrial vegetation, elevated rates of weathering and ephemeral, intense discharge would have persisted. Algeo and Twitchett (2010) studied Early Triassic sediment fluxes from 16 marine Permian-Triassic boundary sections; sediment flux to marine depositional systems increased by an average of 700%. This is attributed to accelerated rates of chemical and physical weathering as a result of the Siberian Traps causing higher surface temperatures, increased acidity of precipitation and changes in landscape

Figure 6.2: Global paleogeography at Permian-Triassic boundary (ca. 252 Ma); E—Ellesmere Island, M—Meishan, PA—Paleo-Arctic Ocean, S—Siberian Traps, SC—South China, Sv—Sverdrup Basin (modified after Algeo et al., 2012).

stability due to the destruction of the terrestrial ecosystem. The sediment flux showed no increase in more distal, deep-sea settings owing to their remoteness from the continental siliciclastic sources. Increased sediment flux during the Early Triassic cannot have been solely from massive soil erosion, which would have accompanied loss of vegetative cover, but would have resulted from increased exposure to bedrock following removal of vegetation and soil (Algeo and Twitchett, 2010). The high sediment flux was sustained for most of the Early Triassic, until the resurgence of forests in the Olenekian. With the elimination of vegetation, braided channels would have been the dominant channel morphology after the late Permian extinction event, and thus if the boundary was conformable, a change in fluvial style should be observed.

In the Karoo Basin of South Africa, there is a basin-wide change from meandering to braided river systems across the Permian-Triassic boundary; this change is consistent with geomorphic consequences from a rapid and major extinction event (Ward et al., 2000). With similarities to the Cape Butler Member, the earliest Triassic sandstone in the Karoo Basin is comprised of erosively based tabular sandstone, horizontally laminated, with numerous patches of maroon mudrock clasts; uneroded tops of these sandstone units display dune forms as indicated by planar cross-bedding with plane-parallel laminations (Ward et al., 2000). The change from meandering to braided system can be triggered by causes other than the removal of vegetation as braided channels can occur on steeper gradients, but there is no record of a major orogenic event in the Karoo Basin. The most probable cause is the extinction event allowing increased sediment delivery into the basin and thus increasing sediment loads in channels creating a braided river system.

The change in fluvial style was recorded in the northern Bowen Basin, Australia. The Lower Triassic basal Sagittarus Sandstone in the Rewan Group is characterised by sheet-like elements, suggestive of broad, shallow channels in a deforested braid-plain setting; the channel deposits represent highly mobile sandy systems, dominated by flashy run-off (Michaelsen, 2002). In comparison, the Late Permian fluvial style is defined by a

Figure 6.3: Summary of architectural models of fluvial styles across the P-T boundary in the northern Bowen Basin; A – Late Permian peatland with major, constrained, trunk river channel systems, banked by extensive tracts of crevasse splay deposits; B – Early Triassic deforested braid plain with unconstrained shallow channels (from Michaelsen, 2002).

trunk river system coupled with low sinuosity due to the stabilising effect of vegetation adjacent to the channel, specifically peat-forming plants, which did not recover in the basin until 6 million years after the extinction event (Michaelsen, 2002). Figure 5.3 illustrates the change in fluvial style across the boundary with the Early Triassic schematic comparable to the Bjorne model. As in the Karoo Basin, the Bowen Basin has been affected by the mass extinction of plants which altered the style of sedimentation.

Michaelsen (2002) documented sandstone petrology across the boundary and found that the Triassic sandstone showed a substantial decrease in feldspars and enrichment in quartz relative to the Late Permian sandstone; this could be linked to elevated rates of chemical weathering. Algeo et al. (2012) documented a change in petrology in the Sverdrup Basin from the Lindström Formation into the Blind Fiord Formation and found a shift in the composition of the detrital fraction; they inferred that it reflects a gradual increase in subaerial weathering intensity rather

than a change in provenance. This is congruent with the data from Sm-Nd isotopes (Patchett et al., 2004), which show a consistent cover of sediment over the Precambrian Shield from the Carboniferous to Tertiary. There is no petrology data from the underlying Trold Fiord Formation to compare with the Bjorne Formation, but with the apparently steady provenance of sediment into the Sverdrup Basin, it can be assumed that any change in petrology would be due to weathering rather than a change in provenance.

Michaelsen (2002) and Ward et al. (2000) reported an increase in sediment flux across the boundary; however, the Bowen Basin received 70 m/Myr in the Upper Permian and 78.5 m/Myr in the Lower Triassic which is substantially lower than the 700% increase that Algeo and Twitchett (2010) proposed. Within the latest Permian interval of the West Blind Fiord study section on Ellesmere Island, sedimentation rates increased by a factor of 3.5×, from 25 to 88 m/Myr, and even higher sediment fluxes characterized the Lower Triassic of the northern Pangean margin (Algeo et al., 2012). Based on a provisional analysis of linear sedimentation rates (LSR) and bulk accumulation rates (BAR) in the Early Triassic based on the measured sections (Tables 6.1 and 6.2), it is evident that the sediment flux changed dramatically during this period. The percent increases in sediment flux are also significantly larger than the global average of 700% across the boundary. This could be due to the proximity to the Siberian Traps as well as the effect of the Arctic Extinction Event increasing the amount of weathering. The data shows a decrease in sediment flux further from the Permian-Triassic boundary, consistent with a slow recovery of terrestrial vegetation. Similar LSR values are reported from Meishan in China (location in Fig. 6.2). The sedimentation rate in the Griesbachian was 110 m/Myr, in the Dienerian was 488 m/Myr and in the Smithian-Spathian/Olenekian was 105m/Myr (Algeo and Twitchett, 2010). The total thickness of strata in the Sverdrup Basin is 13,000 m, and according

	Thickness (m)	Age	Duration (Myr)	LSR (m/Myr)	BAR (g m-2 yr)
Bjorne Fm	1020	Griesbachian - Spathian	5.6	182	455
Cape O'Brien Mbr	300	Smithian - Spathian	3.2	94	235
Pell Point Mbr	280	Smithian	1.1	255	637.5
Cape Butler Mbr	240	Griesbachian - Dienerian	0.9	267	667.5
Lindström Formation	20	Changhsingian	3.4	5.9	14.7

Table 6.1: Linear sediment rates (LSR) and bulk accumulation rates (BAR) for members of the Bjorne Fm using thickness values from measured section. Lindström Formation data is taken from West Blind Fiord (Grasby and Beauchamp, 2009). See appendix C for comparison to global values (data from Algeo and Twitchett, 2010).

	LSR %	BAR %
Changhsingian – Griesbachian	4520%	4541%
Changhsingian - Spathian	3087%	3095%

Table 6.2: Percent change from latest Permian to earliest Triassic (Griesbachian) to late Early Triassic (Spathian).

to the Lower Triassic isopach map, both the Fosheim and Melville depocentres accumulated over 2,000 m of siliciclastics. That is equivalent to 15% of the total strata in the basin, amassed in ~5.6 Myr, corresponding to 2% of the duration of sediment accumulation from the Early Carboniferous to the Paleogene (~280 Myr). The ~1,000 m of Lower Triassic strata in the Sawtooth Range study area is equivalent to 8% of the total basinal strata.

The extinction events were very likely an important factor in the increase in sedimentation to the basin in Early Triassic and were responsible for the dominance of braided stream facies on the basin margin. Supplementary to this theory, it can be suggested that tectonic uplift of the cratonic areas related to the major global tectonic event at the end of the Permian (the Siberian

traps being a part of this major tectonic episode) was a significant cause of the greatly increased sediment flux (Embry, pers. comm., 2012).

That was clearly a time of anomalous sediment flux which is interpreted to be the result of the Latest Permian Extinction and to a lesser extent the Arctic Extinction Event. From provenance studies, it is known that there was an abundant supply of sediment to the south east of the basin in the form of the Devonian Clastic Wedge, and after the Permian-Triassic boundary, bedrock would have been exposed after massive soil erosion. With the prevalent atmospheric conditions from the Siberian Traps volcanic eruptions increasing both chemical and physical weathering, accelerated bedrock weathering would have caused the rapid shedding of the siliciclastics covering the Shield. With a reduction in the vegetation stabilizing banks, there would have been an increase in bedload transported into the basin by broad, shallow, ephemeral, braided rivers. The sand sheets would have extended into the marine environment forming a braid-delta, typically found before the evolution of plants and resembling Miall's (1996) distal braidplain model (Eriksson et al., 1995). The architecture and sedimentary structures observed in the Bjorne Formation indicate rapid, pulsatory flow which is common in fluvial/deltaic systems in the absence of rooted plants. From previous studies of the effect of the Permian-Triassic boundary on sedimentation style, it can be strongly suggested that the anomalous sediment supply in the Sverdrup Basin during the Early Triassic was the result of the largest extinction event in geological history.

6.2 Economic Potential

The Sverdrup Basin was drilled from 1969 to 1986, during which 17 oil and/or gas fields were discovered from a total of 120 drilled wells. The drilling of the Bjorne Formation has been limited in the eastern Sverdrup Basin compared to the central and western region of the basin.

Given that the Bjorne Formation is 1,000 m thick in the study area and greater than 2,000 m thick in the depocentres, it is important to know if it can be interpreted as a reservoir rock. In order for the Bjorne Formation to be evaluated as prospective, it needs to be an effective reservoir and have a source, trap and seal.

Hydrocarbons have been previously discovered in Lower Triassic sandstones in the Arctic. In central Sverdrup Basin, the Marie Bay oil sand deposit, representing an exhumed oil field on the basin flank, is exposed as part of the Bjorne Formation on Melville Island. Contemporaneous with the Bjorne Formation is the super giant Prudhoe Bay oil field in northern Alaska (Fig. 6.4). The primary producing unit, the Lower Triassic Ivishak Sandstone, a fluviodeltaic facies, delivered 1.45 million barrels a day in the 1980's (Atkinson et al., 1990). The Ivishak Sandstone was deposited in a similar paleogeographic setting as the Bjorne Formation when Alaska is repositioned before it was rotated by the opening of the Canada Basin. The source rock overlies the Ivishak Sandstone and hydrocarbons migrated stratigraphically downwards due to the presence of anticlinal structures.

The scarcity of feldspars and lithic fragments in the Bjorne Formation is desirable for sandstone reservoirs as these grains readily decompose and can be easily deformed during compaction thereby decreasing porosity and permeability. The study area is in one of the prospective areas in the Sverdrup Basin for hydrocarbons due to thickness and positive values for porosity and permeability (see Section 5.3). From petrographic and electron microprobe data, carbonate cement is ubiquitous throughout the Bjorne Formation; the calcite cement is interpreted to be pore-filling during early diagenesis which might occlude most of the porosity, similar to the sandstone reservoir of the South Gabon rift basin (Giroir et al., 1989).
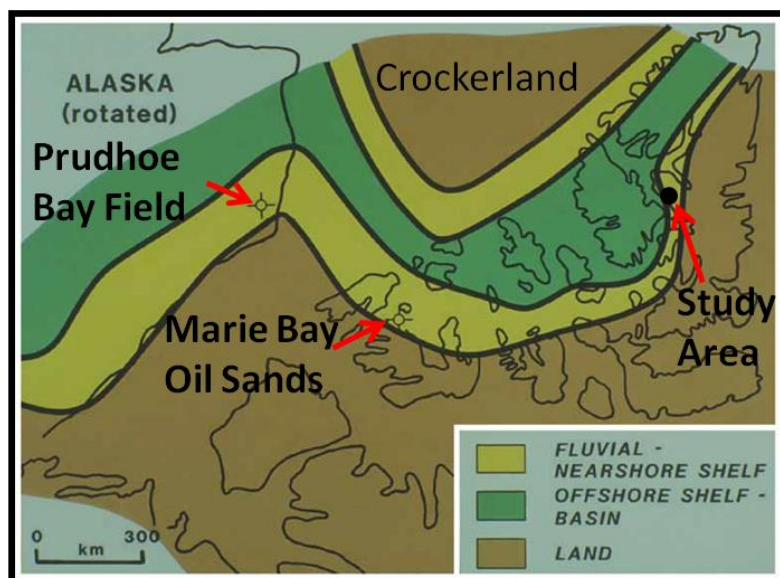
Figure 6.4: Paleogeography of Early Triassic with pre-drift location of Alaska, showing proven and prospective Early Triassic hydrocarbon reservoirs (modified after Embry, 2009).

The level of thermal maturation in the Bjorne Formation is consistent with the generation of hydrocarbons during burial. As a large sandstone unit, it is unlikely to have had suitable source rocks to generate oil or gas, but there are shale-rich units, like the Blind Fiord and Murray Harbour formations and in the Lower Paleozoic, like the van Hauen Formation. Hydrocarbons might also have migrated up-dip from rock units in the more mature basin centre. An issue for Lower Triassic shale is that it may have had a reduced organic content due to the extinction event; however it is possible that the Svartfjeld Member had enough organics to produce hydrocarbons as the recovery of microfaunal and macrofaunal had begun before the Spathian (Fig. 6.1).

The overlying Murray Harbour Formation is identified as a prolific source rock. The bituminous shale contains abundant (up to 10% total organic carbon) Type II kerogen and has excellent hydrocarbon yields in the mature zone (Embry et al., 1991). Hydrocarbon generation in the Murray Harbour shale took place during the Late Cretaceous in the axis of the basin, and further west, generation occurred in the Tertiary. The majority of hydrocarbons in the Sverdrup Basin, regardless of geographic position, are from the shales of the Middle Triassic Murray Harbour or Upper Triassic Hoyle Bay formations, indicating considerable vertical and lateral migration; however, the formations show considerable variation in maturity level (Embry et al.,

1991). Few wells have penetrated the Lower Paleozoic strata, so the thermal maturity and source rock quality is largely uncertain. Oil shows have been observed in the van Hauen Formation suggesting an oil-prone source rock in the succession and most Upper Paleozoic strata are in the mature zone along the margins (Embry et al., 1991).

Potential traps in the Bjorne Formation include Tertiary anticlines, salt structures and structural- stratigraphic traps associated with unconformities on the basin margin or basinward facies change. The main play in the Sverdrup Basin occurs in the Tertiary structures, due to the Eurekan Orogeny, and all the discovered hydrocarbon pools occur in these traps (Embry and Beauchamp, 2008). For the Bjorne Formation, structural-stratigraphic traps would be the most prospective along the eastern margin of the basin. There are two possible seals from the Smith Creek and Svartfjeld transgressive shale/siltstone members. The excellent source rock from the Murray Harbour Formation directly overlies the Bjorne Formation, providing a seal.

Since the study area is along the margin of the basin, unconformity traps are a possibility, and are the traps for hydrocarbons in the Bjorne Formation on Melville Island. There are an abundance of traps associated with salt diapirs such as overturned sediment, strata-flanking unconformities, rim synclines, and salt wings (Embry, 2011); however, the diapirs are predominantly situated along the axis of the basin, and with the Bjorne Formation flanking the margins of the basin, there is minimal opportunity for diapir-related traps to form in the Bjorne
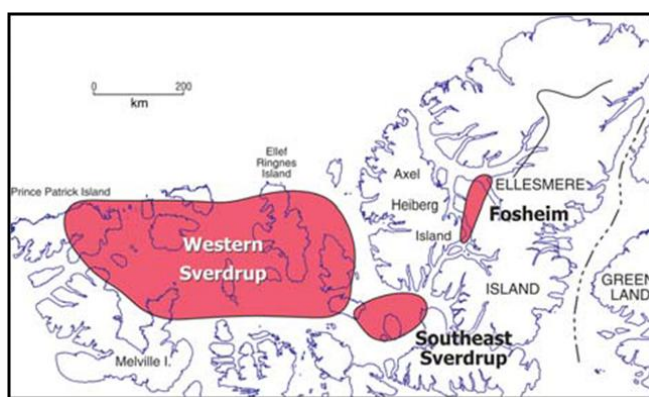
Figure 6.5: Prospective areas for hydrocarbon fields in Triassic–Jurassic strata (from Embry, 2011).

Formation. In the Fosheim prospective area (Fig. 6.5), the wells encountered thick fluvial sandstones that change facies to shale and siltstone westward, and it is possible that a stratigraphic component will be a part of traps involving Lower Triassic strata in the western portion of the area (Embry, 2011).

The composition, thermal maturation, permeability levels, reservoir thickness, seal and possible source rocks make the Bjorne sandstone a prospective reservoir. The early pore-filling calcite cement occludes porosity, dissolution of grains opened up secondary porosity, late stage ferroan-dolomite-ankerite replaced the calcite, and infilled secondary pore space. Later veining and fracturing could provide increased porosity. Porosity values from core analysis and point count vary slightly, but the best reservoir would be the Cape O'Brien Member as it appears to have substantially higher porosity and has undergone less burial than the other two members.

CHAPTER 7: CONCLUSIONS AND RECOMMENDATIONS

7.1 Sedimentological Results

Reconnaissance mapping enabled the construction of a detailed section to identify sedimentology and lithofacies, which aided in constraining a depositional model for the Lower Triassic Bjorne Formation. The lowermost member, the Cape Butler Member, is composed primarily of sandstones with upper flow regime plane beds that display rapid transition to lower flow regime bedforms, mainly ripples. Cross-beds formed by fluvial dunes are scarce and thin red siltstones cap some waning-flow successions. The middle Pell Point Member is dominated by dune cross-stratification, with some parallel lamination. The uppermost member, Cape O'Brien, is similar to Pell Point, with a large occurrence of dune cross-stratification. Additional structures include bedforms in the upper/lower regime transition, antidune bedding, one possible chute-and-pool structure, and many erosional surfaces, many of which are lagged with intraclasts. The lower two members have mudstone rip-up clasts, and the upper Cape Butler and Cape O'Brien members have extra-formational clasts.

In their architecture, sandstone units are laterally extensive, multistory, and stacked in units a few metres thick, with relatively little indication of major channel forms. Plant fragments are very rare. The Bjorne Formation was an ephemeral depositional system subject to repeated intense floods that laid down sufficient sand and waned sufficiently rapidly to preserve high flow-strength bedforms. There is evidence of sub-aqueous conditions with the presence of synaeresis cracks and trace fossils, mostly in the Cape Butler Member, including *Skolithos, Diplocraterion, Thalassinoides, Palaeophycus,* and *Arenicolites*. Although non-diagnostic of a specific environment, their presence suggests marine influence at some levels and are indicative

of behaviour representative of the depositional conditions at the time. The braided fluvial system

passed basinward into a marine-influenced environment, and can be classified as a braid-delta.

7.2 Cause of Rapid Sedimentation

Deposition took place immediately following the Permo/Triassic boundary with its major

extinction event. The reduction in diversity of vegetation and likely reduction of vegetation cover

may have enhanced sediment loading, and the absence of channel bank stability may have

promoted the development of broad bedload channels. With the bulk of the mud that passed

through the system deposited in the Blind Fiord Formation, and considering also the low amount

of mud in the Bjorne Formation and the decrease of channel bank stability, sediment dynamics

within braided ephemeral and tidal/ subtidal channels of a braid-delta would have resembled in

some respects strata architecture found before the evolution of plants, promoting the formation of

extensive sandstone sheets. The sediment flux from the Changhsingian to Griesbachian increased

4541%, well above the global sediment flux across this boundary, which has an average increase

of 700%. This anomalous sedimentation could be due in part to the proximity to the Siberian

Traps, which may have increased the acidity of precipitation and rates of chemical and physical

weathering, as well as affecting terrestrial ecosystems. The early-stage eruptions caused the

Arctic Extinction Event, with the main-stage eruption causing the catastrophic Late Permian

Extinction.

7.3 Diagenesis and Economic Potential

Petrographic analysis identifies the Bjorne Formation as a quartzarenite to sublitharenite with

abundant carbonate cement, comprising of early, pore-filling calcite, and late, grain-replacive

dolomite-ankerite rhombohedra. The calcite cement occluded most of the porosity, but later grain

dissolution and fracturing secondary porosity, which was occluded by dolomite-ankerite

rhombohedra. Very general burial temperatures are assumed by comparison with the Gulf of Mexico, a first-cycle basin, where early, pore-filling calcite occurs within the range of 20-70°C, and late-stage replacement of calcite by ankerite occurs within the range of 80-145°C. The Cape O'Brien Member is the most prospective member because it has higher porosity (~22%) and has not been affected by burial to the same extent as the lower two members. From core analysis, the permeability and porosity are, on average, very good and good, respectively; however, point count methods provide lower porosity values for the lower two sandstone members. In the study area, the Bjorne sandstone lies in the oil window, interpreted from vitrinite reflectance data, and has source rocks of Triassic shales and potential seals from shale tongues. The provenance of the sediment is determined as from the craton interior and recycled orogen. From previous studies, the Shield was covered in Devonian siliciclastics sourced from the Caledonian and Ellesmerian orogens which supplied the bulk of sediment for the south and east margins of the basin.

7.4 Recommendations for Further Analysis

The Bjorne Formation is extensive around the southern and eastern margins of the Sverdrup Basin, and a much more comprehensive study needs to be undertaken in order to fully understand the Lower Triassic strata. The following measures are recommended:

1. Extensive field work should be conducted to determine if the sedimentology and facies associations are laterally continuous, and more detailed sedimentology would benefit the current interpretation. Field work should also be carried out on Melville Island to compare the southern margin to the eastern margin as there might be distinguishing characteristics, or it could investigate further the evidence for ephemeral sedimentation provided in this study. Extensive field work could explain the sedimentation and depositional environment on a basinal scale for a critical moment in the history of the

Sverdrup Basin, as well as better understanding the impact of the Late Permian

Extinction.

2. The petrology of the Bjorne Formation was unknown before this study, which is largely

    qualitative and preliminary. There is an interesting diagenetic and mineralogical story,

    and systematic sampling would be needed to understand the differences between the

    members. Greater use of the electron microprobe would be useful to track the changes in

    the elemental composition of carbonate cements, and to better understand the relationship

    between burial history and cementation events. Quantitative analysis should be used to

    constrain the bulk composition values and correlate to stratigraphic level in the measured

    section.

3. Polished thin sections could be made for cathodoluminescence (CL) analysis of carbonate

    minerals and feldspars and would further the understanding of the diagenetic timing. CL

    analysis of feldspars could be used to recognize albitization of feldspars. Also, CL

    analyses for carbonates are used to recognize and divide the stages and types of carbonate

    cementation. This could assist in quantifying the types of calcite and ankerite-dolomite to

    better understand a correlation to stratigraphic level in the measured section.

4. Samples from the Blind Fiord Formation or shale members in the Bjorne Formation

    should be analyzed for total organic carbon, to determine if the shale is truly devoid of

    organics, or perhaps if it is rich in a mono-specific assemblage.

5. More thin sections can be stained with blue epoxy systematically throughout each

    member to constrain the average and maximum porosity values to better compare to the

    data from core analysis. Using software to quantify the porosity would provide more

    accurate numbers than the point count method used here. A better understanding of the

type and percentage of porosity would greatly benefit in constraining the economic

potential.

6. The petrography could be complemented by scanning electron microscope (SEM), X-ray

diffraction (XRD) and isotopic analysis for oxygen and carbon in carbonates. SEM could

be used for finding evidence of grain dissolution and identification of clay types. XRD

can be used to determine the clay mineralogy as the type of clay was not able to be

identified in thin section or electron microprobe. Isotopic signatures of the cementing

phases could provide information about the sources for the carbon and oxygen. This

would greatly assist in unravelling the diagenetic history.

REFERENCES

Adams, A.E., MacKenzie, W.S., and Guilford, C. 1984. Atlas of Sedimentary Rocks Under the Microscope. Longman Scientific & Technical, Essex, England.

Algeo, T., Henderson, C.M., Ellwood, B., Rowe, H., Elswick, E., Bates, S., Lyons, T., Hower, J.C., Smith, C., Maynard, B., Hays, L.E., Summon, R.E., Fulton, J., and Freeman, K.H. 2012. Evidence for a diachronous Late Permian marine crisis from the Canadian Arctic region, Geological Society of America Bulletin, doi: 10.1130/B30505.1.

Algeo, T.J., and Twitchett, R.J. 2010. Anomalous Early Triassic sediment fluxes due to elevated weathering rates and their biological consequences. Geology, 38: 1023–1026.

Allen, J. R.L. 1973. A classification of climbing ripple cross-lamination. J. Geol, Soc, London, 129: 537-541.

Ashley, G.M., Southard, J.B., and Boothroyd, J.C. 1982. Deposition of climbing-ripple beds: a flume simulation. Sedimentology, 29 (1): 67– 79.

Atkinson, C.D., McGowen, J.H., Bloch, S., Lundell, L.L., and Trumbly, P.N. 1990. Braidplain and deltaic reservoir, Prudhoe Bay field, Alaska. *In*: Sandstone Petroleum Reservoirs, Barwis, J.H., McPherson, J.G., Studlick, J.R.J. and Ginsburg, R.N., (eds.), United States: Springer-Verlag, New York, NY, United States, 7-29.

Balkwill, H.R., 1978. Evolution of Sverdrup Basin. AAPG Bulletin, 62: 1004–1028.

Beauchamp, B., Henderson, C.M., Grasby, S.E., Gates, L.T., Beatty, T.W., Utting, J., and James, N.P. 2009. Late Permian sedimentation in the Sverdrup Basin, Canadian Arctic: The Lindström and Black Stripe Formations. Bulletin of Canadian Petroleum Geology, 57: 167–191.

Christie, R.L., Embry, A.F., and Van Dyck, G.A. 1981. Lexicon of Canadian Stratigraphy; Vol. 1, Arctic Archipelago (District of Franklin), Canada. Canadian Society of Petroleum Geologists, Calgary, AB, Canada.

Dalrymple, R.W., and Choi, K. 2007. Morphologic and facies trends through the fluvial-marine transition in tide-dominated depositional systems: A schematic framework for environmental and sequence-stratigraphic interpretation. Earth-Science Reviews, 81 (3-4): 135-174.

Davies, N.S., and Gibling, M.R. 2010. Cambrian to Devonian evolution of alluvial systems: The sedimentological impact of the earliest land plants. Earth-Science Reviews, 98: 171–200.

Deer, W.A., Howie, R.A., and Zussman, J. 1970. An Introduction to the Rock-forming Minerals. Longman, London.

Dickinson, W.R., and Suczek, C.A. 1979. Plate tectonics and sandstone composition. AAPG Bulletin, 63: 2164-2182.

Dickinson, W. R., Beard, L. S., Brakenridge, G. R., Erjavec, J. L., Ferguson, R. C., Inman, K. F., Knepp, R.A., Lindberg, F.A., and Ryberg, P. T. 1983. Provenance of North American Phanerozoic sandstones in relation to tectonic setting. Geological Society of America Bulletin, 94(2): 222-235.

Embry, A.F. 1986. Stratigraphic subdivision of the Blind Fiord and Bjorne formations (Lower Triassic), Sverdrup Basin, Arctic Islands. Current Research, Part B, Geological Survey of Canada, paper 86-1B: 329–340.

Embry, A.F. 1988. Middle-Upper Devonian sedimentation in the Canadian Arctic Islands and the Ellesmerian Orogeny. *In*: McMillan, N. J.; Embry, A. F.; and Glass, D. J., (eds.), Devonian of the world, Vol. 2, CSPG Memoir, 14: 15–28.

Embry, A.F. 1993. Crockerland – the northern source area for the Sverdrup Basin, Canadian Arctic Archipelago. *In*: Vorren, T., Bergsager, E., Dahl-Stamnes, O., Holter, E., Johansen, B., Lie, E., and Lund, T., (eds.), Arctic Geology and Petroleum Potential, Norwegian Petroleum Society, Special Publication no. 2: 205–216.

Embry, A.F. 2009. Lower Triassic Stratigraphy and Petroleum Potential, Sverdrup Basin, Arctic Canada. Oral Presentation, AAPG Convention, Denver, Colorado, June 7-10, 2009

Embry, A.F. 2011. Petroleum prospectivity of the Triassic–Jurassic succession of the Sverdrup Basin, Canadian Arctic Archipelago. *In*: Spencer A. M., Embry A. F., Gautier D. L., Stoupakova A. V., Sørensen K., (eds.), Arctic Petroleum Geology, Memoirs of the Geological Society of London, 35: 545–558.

Embry, A.F., and Beauchamp, B. 2008. Sverdrup Basin. *In*: Hsü, K.J. (ed.), Sedimentary Basins of the World, Vol. 5, The Sedimentary Basins of the United States and Canada, Andrew D. Miall. The Netherlands: Elsevier, 451 – 471

Embry, A.F., Powell, T.G., and Mayr, U. 1991. Petroleum resources, Arctic Islands. *In*: Chapter 20 of Geology of the Innuitian Orogen and Arctic Platform of Canada and Greenland, Trettin, H.P., (ed.), Geological Survey of Canada, Geology of Canada no. 3 (also Geological Society of America, The Geology of North America, v. E)

Eriksson, P.G., Reczko, B.F.F., Boshoff, A.J., Schreiber, U.M., Van der Neut, M., and Snyman, C.P. 1995. Architectural elements from Lower Proterozoic braid-delta and high-energy tidal flat deposits in the Magaliesberg Formation, Transvaal Supergroup, South Africa. Sedimentary Geology, 97: 99–117.

Fielding, C.R. 2006. Upper flow regime sheets, lenses and scour fills: Extending the range of architectural elements for fluvial sediment bodies. Sedimentary Geology, 190: 227-240.

Folk, R.L. 1974. Petrology of sedimentary rocks. United States: Hemphill, Austin, Texas

Gouramanis, C., Webb, J.A., and Warren, A.A., 2003. Fluviodeltaic sedimentology and ichnology of part of the Silurian Grampians Group, western Victoria. Australian Journal of Earth Sciences, 50, pp. 811-825.

Grasby, S.E., and Beauchamp, B., 2009. Latest Permian to Early Triassic basin-to-shelf anoxia in the Sverdrup Basin, Arctic Canada. Chemical Geology, 264, pp. 232-246.

Grasby, S.E., Sanei, H., and Beauchamp, B. 2011. Catastrophic dispersion of coal fly ash into oceans during the latest Permian extinction. Nature Geoscience, 4: 104–107.

Harrison, J.C., 2005. Geological history of the Arctic. *In*: Nuttall, M., (ed.), Encyclopedia of the Arctic. Routledge, New York, 711-722.

Hayes, M.J., and Boles, J.R. 1993. Evidence for meteoric recharge in the San Joaquin basin, California provided by isotope and trace element chemistry of calcite. Journal of Marine and Petroleum Geology, 10: 135–144.

Hu, K., and Dewing, K., 2011. Geological and geochemical data from the Canadian Arctic Islands. Part X: Core petrophysical data from petroleum exploration boreholes. Geological Survey of Canadda Open File 6669 (CD-ROM).

Irving, E., and Irving, G.A. 1982. Apparent polar wander paths Carboniferous through Cenozoic and the assembly of Gondwana. Geophysical Surveys, 5: 141–188.

Kearsey, T., Twitchett, R.J., Price, G.D., and Grimes, S.T. 2009. Isotope excursions and palaeotemperature estimates from the Permian/Triassic boundary in the Southern Alps (Italy). Palaeogeography, Palaeoclimatology, Palaeoecology, 279: 29–40

Kim, J. C., Lee, Y. I., and Hisada, K. 2007. Depositional and compositional controls on sandstone diagenesis, the Tetori Group (Middle Jurassic-Early Cretaceous), Central Japan. Sedimentary Geology, 195(3-4): 183-202.

Long, D.G.F. 2011. Architecture and depositional style of fluvial systems before land plants; a comparison of Precambrian, Early Paleozoic, and modern river deposits. Special Publication - Society for Sedimentary Geology, 97(1060-071): 37-61

Looy, C.V., Brugman, W.A., Dilcher, D.L., and Visscher, H. 1999. The delayed resurgence of equatorial forests after the Permian-Triassic ecological crisis. Proceedings of the National Academy of Sciences of the United States of America, 96: 13,857–13,862

MacEachern, J.A., Pemberton, S.G., Gingras, M.K., and Bann, K.L. 2010. Ichnology and Facies Models. *In*: Dalrymple, R.W., and James, N.P., (eds.), Facies Models, edition 3: Geological Association of Canada, St. John's Newfoundland: 19-58.

McBride, E.F. 1963. A classification of common sandstones. Journal of Sedimentary Petrology, 33: 664–669.

McKee, E.D. Crosby, E.J., and Berryhill, H.L., 1967. Flood deposits, Bijou Creek, Colorado. Journal of Sedimentary Petrology, 37: 829–851.

Miall, A.D. 1990. Principles of Sedimentary Basin Analysis, 2nd Edition: New York, Springer-Verlag.

Miall, A.D. 1996. The Geology of Fluvial Deposits, Springer, Berlin

Michaelsen, P. 2002, Mass extinction of peat-forming plants and the effect on fluvial styles across the Permian-Triassic boundary, northern Bowen Basin, Australia. Palaeogeography Palaeoclimatology, Palaeoecology, v. 179, 173–188

Miller, E.L., Toro, J., Gehrels, G., Amato, J.M., Prokopiev, A., Tuchkova, M.I., Akinin, V.V., Dumitru, T.A., Moore, T.E., and Cecile, M.P. 2006. New insights into Arctic paleogeography and tectonics from U–Pb detrital zircon geochronology. Tectonics, 25. doi:10.1029/ 2005TC001830.

Miller, M.F. 1984. Distribution of biogenic structures in Paleozoic non-marine and marine-margin sequences. An actualistic model: Journal of Paleontology, 58: 550-570.

Nassichuk, W.W., Thorsteinsson, R. and Tozer, E.T. 1973. Permian–Triassic boundary in the Canadian Arctic Archipelago. *In*: Logan, A., Hills, L.V., (eds.), The Permian and Triassic Systems and Their Mutual Boundary. CSPG Memoir, 2: 286–293

Nesse, W.D. 1986. Introduction to optical mineralogy. New York: Oxford University Press.

North, F K. 1985, Petroleum geology. United States: Allen & Unwin, Boston, MA, United States

Okulitch, A.V. (compiler). 1991. Geology of the Canadian Archipelago and North Greenland; Figure 2. *In*: Trettin H.P., (ed.), Innuitian Orogen and Arctic Platform; Canada and Greenland, Geological Survey of Canada, Geology of Canada, No. 3 (*also* Geological Society of America, The Geology of North America, v. E), scale 1:2,000,000

Olairu, C., and Bhattacharya, J.P. 2006. Terminal distributary channels and delta front architecture of river-dominated delta systems, Journal of Sedimentary Research, 76: 212– 233.

Olariu, C., Bhattacharya, J.P., Xu, X., Aiken, C.L.V., Zeng, X., and McMechan, G.A. 2005. Integrated study of ancient delta front deposits, using outcrop, ground penetrating radar and three dimension photorealistic data: Cretaceous Panther Tongue sandstone, Utah. *In*: Giosan, L., and Bhattacharya, J.P., (eds.), River Deltas: Concepts, Models, Examples: SEPM, Special Publication 83: 155–178.

Patchett,P.J., Embry, A.F., Ross, G.M., Beauchamp, B., Harrison, J.C., Mayr, U., Isachsen, C.E., Rosenberg, E.J., and Spence, G.O. 2004. Sedimentary cover of the Canadian Shield through Mesozoic time reflected by Nd isotopic and geochemical results for the Sverdrup Basin, Arctic Canada. J. Geol., 112: 39–57.

Pemberton, S.G., Spila, M., Pulham, A.J., Saunders, T., MacEachern, J.A., Robbins, D., and Sinclair, I.K. 2001. Ichnology and sedimentology of shallow to marginal marine systems. Geological Association of Canada, Short Course Notes 15.

Picard, M.D., and High, L.R. 1973. Sedimentary structures of ephemeral streams. Developments in Sedimentology. 17. Elsevier, Amsterdam.

Plummer, R.S., and Gostin, V.A. 1981. Shrinkage cracks: desiccation or synaeresis. Journal of Sedimentary Petrology, 51: 1147-1156.

Poursoltani, M. R. and Gibling, M. R. 2011. Composition, porosity, and reservoir potential of the middle Jurassic Kashafrud Formation, northeast Iran. Marine and Petroleum Geology, 28(5): 1094-1110.

Retallack, G.J. 1995, Permian-Triassic extinction on land. Science, 267: 77–80.

Retallack, G.J. 1999. Postapocalyptic greenhouse paleoclimate revealed by earliest Triassic paleosols in the Sydney Basin, Australia. Geological Society of America Bulletin, 111: 52–70.

Røe, S.-L., and Hermansen, M. 1993. Processes and products of large, Late Precambrian sandy rivers in northern Norway. Special Publication of the International Association of Sedimentologists, 17: 151-166.

Roy, K.J. 1972. Bjorne Formation (Lower Triassic), western Ellesmere Island. *In*: Report of Activities, Geological Survey of Canada, Paper 72-1A: 224-246.

Rust, B.R. 1984. Proximal braidplain deposits in the Middle Devonian Malbaie Formation of Eastern Gaspé, Quebec, Canada. Sedimentology, 31: 675-695.

Smith, D.G. 1976. Effect of vegetation on lateral migration of anastomosed channels of a glacial meltwater river. Geological Society of America, Bulletin, 87: 857-860.

Southard, J.B., and Boguchwal, L.A. 1990. Bed configuration in steady unidirectional water flows; part 2, synthesis of flume data. Journal of Sedimentary Petrology, 60(5): 658-679.

Stear, W.M. 1983. Morphological characteristics of ephemeral stream channel and overbank splay sandstone bodies in the Permian Lower Beaufort Group, Karoo Basin, South Africa. *In*: Collinson, J.D., and Lewin, J., (eds.), Modern and Ancient Fluvial Systems, International Association of Sedimentologists, Special Publication 6: 405-420.

Stear, W.M. 1985. Comparison of the bedform distribution and dynamics of modern and ancient sandy ephemeral flood deposits in the southwestern Karoo region, South Africa. Sedimentary Geology, 45: 209-230.

Steefel, C.I. 2008, Geochemical Kinetics and Transport. *In*: Brantley, S.L., Kubicki, J.D., and White, A.F., (eds.), Kinetics of Water-Rock Interaction, Springer, New York, 545-589.

Tozer, E.T. 1963. Blind Fiord. *In*: Geology of the north central part of the Arctic Archipelago, Northwest Territories (Operation Franklin). Geological Survey of Canada, Memoir 320: 380-385.

Tucker, M.E. 1991. Sedimentary Petrology. Blackwell, Oxford.

Waples, D.W. 1980. Time and temperature in petroleum formation; application of Lopatin's method to petroleum exploration. AAPG Bulletin, 64(6): 916-926.

Ward, P.D., Montgomery, D.R., and Smith, R. 2000. Altered river morphology in South Africa related to the Permian-Triassic extinction. Science, 289: 1740–1743.

Wignall, P.B. 2007. The end-Permian mass extinction—How bad did it get? Geobiology, 5: 303–309.

APPENDIX A: STRATIGRAPHIC COLUMN WITH SAMPLE LOCATIONS
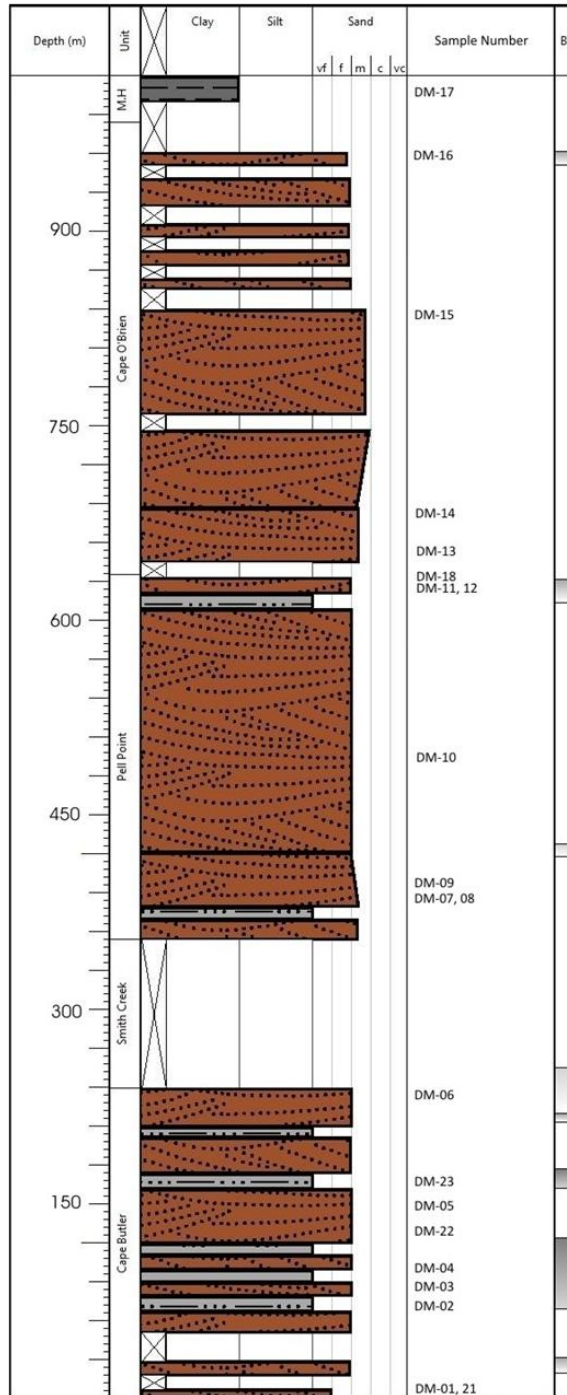
Stratigraphic column, illustrating where samples were taken in relation to stratigraphic level of detailed section; samples DM-19 and -20 were taken away from the measure section and represents the base of Cape Butler Member or, less likely, the Confederation Point Member.

APPENDIX B: BULK MINERALOGY

Sample No.	Unit	Depth (m)	Sorting	Avg Qz G.s (mm)	Quartz (Mono)	Poly	Chert	K-Spar	Plag	Ign	Meta	Musc	Carb.	Misc	Misc. Min
DM-19	Blind/Butler	-	well	<0.05	20								80	-	zr, trm
DM-20	Blind/Butler	-	-	<0.05	55							5	40	-	trm
DM-01	Cape Butler	1	-	-										-	
DM-21	Cape Butler	6	well	<0.05	70							15	15		
DM-02	Cape Butler	79	very well	0.1	70	0	2	1	1	2	2	2	15	-	apt, zr
DM-03	Cape Butler	88	well	0.1	70	2	2	0	1	0	2	2	20		zr
DM-04	Cape Butler	98													
DM-22	Cape Butler	126													
DM-05	Cape Butler	141	very well	0.1-0.2	65		2		1	2	2	2	25		apt, zr, trm
DM-23	Cape Butler	172	well	0.05-0.1	65	1	2	1	1	3	2	5	20	-	apt, zr
DM-06	Cape Butler	236	very well	0.2	55	2	2	1	1		2	1	35		apt, trm
DM-07a	Pell Point	375	well	0.1	45	2	0	1	1	1	1	3	45	2	zr, mnz
DM-07b	Pell Point	375	well	0.2-0.3	80	1	1		1		1	1	15		zr
DM-08	Pell Point	386	very well	<0.05	60							15	15	-	
DM-09	Pell Point	400	well	0.1-0.3	55	1	1		1	1	1	5	35	-	zr
DM-10	Pell Point	500	well	0.2-0.4	85	1	2	1	1	2	5	2		1	zr, apt, mnz
DM-11	Pell Point	622	very well	0.1	70		2			2	1	5	20	-	zr, apt
DM-12	Pell Point	624	well	0.05-0.2	45	2	2	1	1	2	1	1	45	-	rutile
DM-18	Pell Point	635	very well	0.1	30	1	1	1	1				65	1	zr, rutile, mnz
DM-13	Cape O'Brien	648	very well	0.1-0.2	60		2		1		1	1	35	-	zr, apt
DM-14	Cape O'Brien	681	moderate	0.2-0.5	50	2	5			1	1	1	40	-	trm, zr
DM-15	Cape O'Brien	838	well	0.2-0.3	65	3	3	1	1	1		1	25		rutile, zr
DM-16	Cape O'Brien	961	moderate	0.1-0.5	60	2	2	1	1	2	1		30	1	zr, rutile, apt
DM-17	Murray Harbour	1019	well	<0.05	40							5	50	5	

Summary of quantitative analysis of bulk mineralogy, sorted by stratigraphic level; apt – apatite, Carb. – carbonate, Ign – igneous fragment, K-spar – potassium feldspar, Meta – metamorphic fragment, mnz – monazite, Musc – muscovite, Plag – plagioclase, Poly – polycrystalline quartz, trm – tourmaline, zr – zircon. Samples DM-19 and -20 were taken away from the measure section and likely represents the base of Cape Butler Member or, less likely, the Confederation Point Member of the Blind Fiord Formation.

APPENDIX C: MICROPROBE ANALYSIS

Sample	K_2O	Cr_2O_3	Na_2O	SiO_2	MnO	CaO	TiO_2	MgO	Al_2O_3	FeO	BaO	Total
Slide DM-09 Dolo Core Pt 1	0.006	0	0	0	0.179	31.795	0	20.672	0	0.739	0	53.391
- Carbonate Rim Pt 2	0.012	0	0	0.041	0.237	29.918	0	13.99	0	11.66	0	55.858
- Feldspar Pt 3	15.539	0	0.406	65.443	0	0.061	0	0	18.514	0.044	0	100.007
- Feldspar Pt 4	14.864	0	0.637	65.349	0	0.004	0	0	18.373	0.032	0	99.259
- Rutile Pt 5	0.109	0.094	0.012	15.834	0	0.134	78.463	0.003	0.217	0.348	0	95.214
- Rutile Rim Pt 6	0.206	0.065	0.02	1.475	0.01	0.353	91.65	0.033	0.447	0.476	0	94.735
- Rhomb Core Pt 8	0.015	0	0	0.017	0.124	35.512	0	22.4	0	0.065	0	58.133
- Rhomb Rim 1 Pt 9	0.01	0	0	0.036	0.255	32.814	0	17.561	0	8.679	0	59.355
- Rhomb Rim 2 Pt 10	0.026	0	0	0.064	0.213	32.165	0	13.03	0.005	14.061	0	59.564
- Rhomb Rim 3 Pt 11	0.016	0	0	0.047	0.235	31.693	0	16.611	0	8.649	0	57.251
- Pyrite Pt 13	0.059	0.251	0.073	0.349	0.101	0.084	0.128	0.056	0.099	57.557	0.263	59.02
- Rhomb Core Pt 14	0.021	0	0	0.064	0.202	33.955	0	20.676	0.01	4.983	0	59.911
- Rhomb Rim 1 Pt 15	0.025	0	0	0.051	0.204	30.692	0	12.925	0	12.822	0	56.719
- Rhomb Rim 2 Pt 16	0.016	0	0	0.044	0.263	30.26	0	14.283	0	9.624	0	54.49
- Rhomb Rim 3 Pt 17	0.022	0	0	0.039	0.21	35.306	0	18.917	0	6.879	0	61.373
- Clay? Pt 18	7.34	0	0.039	51.42	0	0.295	1.399	2.404	25.062	3.213	0	91.172
- Carbonate Pt 19	0.088	0	0	0.401	0.237	29.649	0.003	14.053	0.117	8.941	0	53.489
- Clay? Pt 20	4.776	0	0.023	31.853	0	1.703	0.084	1.389	15.981	1.814	0	57.623
- Calcite Pt 21	0.091	0	0	0.173	0.048	58.741	0	0.187	0.032	0.395	0	59.667
- Feldspar Pt 22	13.565	0	0.929	63.753	0	0.089	0	0	19.231	0.111	2.94	100.618
- Feldspar Pt 23	15.531	0	0.28	65.403	0	0.136	0	0	18.539	0.12	0.17	100.179
- Rutile Pt 24	0.308	0.094	0.05	6.5	0.02	0.638	90.781	0.069	0.84	0.507	0	99.807
- Calcite Pt 25	0.047	0	0	0.217	0.072	61.135	0	0.159	0.02	0.546	0	62.196
- Dolo Core Pt 26	0.017	0	0	0.03	0.102	32.505	0	21.741	0	0.175	0	54.57
- Dolo Rim Pt 27	0.021	0	0	0.076	0.297	37.09	0	17.937	0	5.268	0	60.689
- Aluminium Silicate Pt 28	7.715	0	0.209	47.27	0.044	0.52	0.224	1.64	27.862	2.528	0	88.012
- Dolo Core Pt 29	0.008	0	0	0.023	0.393	33.051	0.012	19.863	0	6.223	0	59.573
- Dolo Rim 1 Pt 30	0.037	0	0	0.172	0.182	32.382	0	21.607	0.012	0.12	0	54.512
- Dolo Rim 2 Pt 31	0.018	0	0.002	0.027	0.193	32.774	0	19.651	0	1.74	0	54.405
- Dolo Rim 3 Pt 32	0.025	0.02	0	0.059	0.281	31.323	0	16.796	0	8.108	0	56.612
- Dolo Rim 4 Pt 33	0.058	0.05	0.013	0.503	0.266	29.385	0.011	12.347	0.164	12.256	0	55.053
- Calcite Pt 34	0.031	0.013	0.007	0.082	0.086	58.351	0.002	0.294	0	0.532	0	59.398
Slide DM-15 calcite pt 01	0.009	0	0.166	0.032	0	51.627	0	0.125	0.023	0.1	0	52.082
- feldspar pt 2	12.324	0	1.439	61.646	0	0.007	0.006	0.004	18.373	0.036	0.706	94.541
- rutile pt 3	0.096	0.006	0.025	52.259	0.009	0.079	42.482	0.045	0.434	0.318	0	95.753
- feldspar pt 4	12.593	0	1.352	61.793	0	0.007	0	0.018	18.347	0.044	0.704	94.858
- dolo core pt 5	0.2	0	0.031	1.882	0.044	29.574	0	19.048	1.063	0.787	0	52.629
- dolo rim pt 6	0.024	0	0.035	2.584	0.194	25.761	0	9.239	0.129	9.853	0	47.819
- dolo pt 7	0.102	0	0.15	4.857	0.187	21.836	0.006	7.905	1.301	13.991	0.02	50.355
- dolo core pt 8	0.076	0	0.027	0.895	0.02	30.174	0	19.183	0.34	0.88	0	51.595
- dolo rim pt 9	0.013	0	0.042	0.212	0.141	40.894	0	6.729	0.069	4.802	0	52.902
- calcite pt 10	0.017	0	0.02	0.054	0.063	53.618	0	0.137	0	0.177	0.02	54.106
- carbonate core pt 11	0.018	0	0.023	0.135	0.059	30.374	0	20.391	0.009	0.453	0	51.462
- carbonate rim 1 pt 12	0.122	0	0.044	11.961	0.191	27.113	0	15.251	0.472	2.827	0	57.981
- carbonate rim 2 pt 13	0.003	0	0.05	0.059	0.292	31.2	0	15.873	0.031	5.374	0	52.882
- calcite pt 14	0.009	0	0.025	0.08	0.179	50.149	0	2.363	0.008	1.689	0	54.502
- feldspar pt 15	13.611	0	0.779	63.643	0	0.01	0.016	0.012	18.416	0.017	0.672	97.176
- dolo pt 16	0.018	0	0.035	1.605	0.267	31.026	0	14.202	0.072	6.879	0.043	54.147
- feldspar pt 17	13.509	0	0.871	63.755	0	0.051	0.018	0.012	18.368	0.062	0.501	97.147
- dolo rim pt 18	0.038	0	0.078	1.759	0.198	24.897	0.002	12.357	0.253	9.988	0	49.57
- calcite pt 19	0.036	0	0.03	0.388	0.044	52.623	0	0.858	0.169	0.339	0	54.487
- calcite pt 20	0.016	0	0.028	3.923	0.079	51.198	0	0.153	0.046	0.271	0.005	55.719
- dolo core pt 21	0.33	0	0.024	1.965	0.088	29.681	0	19.111	0.642	0.832	0	52.673
- 15 dolo rim 1 pt 22	0.031	0	0.061	1.331	0.108	27.299	0	15.608	0.148	5.515	0	50.101
- 15 dolo rim 2 pt 23	0.014	0	0.059	0.624	0.18	26.518	0	11.43	0.119	10.217	0.023	49.184
- 15 dolo rim 3 pt 24	0.022	0	0.049	0.388	0.27	29.265	0	10.513	0.091	12.082	0	52.68
- 15 dolo core pt 25	0.018	0	0.037	0.205	0.078	30.745	0.119	18.814	0.068	1.596	0	51.68
- 15 dolo rim 1 pt 26	0.041	0	0.043	1.026	0.145	31.153	0	17.777	0.223	2.051	0	52.459
- 15 dolo rim 2 pt 27	0.031	0	0.029	0.437	0.213	29.707	0	15.328	0.123	5.156	0	51.024
- 15 dolo rim 3 pt 28	0.029	0	0.051	0.806	0.163	25.416	0	10.801	0.237	11.109	0	48.612
- 15 dolo rim 4 pt 29	0.035	0	0.033	3.194	0.223	25.221	0	9.396	0.235	13.554	0.024	51.915
- 15 calcite pt 30	0.315	0	0.039	40.519	0.054	30.5	0.021	0.22	2.127	0.389	0	74.184
- 15 calcite pt 31	0.015	0	0.007	0.788	0.121	52.531	0.011	0.844	0	1.097	0	55.414
- 15 feldspar pt 32	12.721	0	0.437	61.193	0.017	0.085	0.022	0.032	17.842	0.23	0.725	93.304
- 15 feldspar pt 33	12.888	0	0.425	61.161	0.024	0.075	0.013	0.032	17.782	0.245	0.678	93.323

Table of electron microprobe data, values are not normalized. Carbon was not measured, which will affect total values, specifically carbonates.

APPENDIX D: LSR AND BAR DATA

Locality	Changhsingian			Griesbachian			Gr/Ch	Ch	Gr	Gr/Ch
	Thickness (m)	Duration (Myr)	LSR (m/Myr)	Thickness (m)	Duration (Myr)	LSR (m/Myr)	LSR %	BAR (g m^{-2} yr^{-1})	BAR (g m^{-2} yr^{-1})	BAR %
Chaohu, Anhui	48	3.4	14.1	60	0.7	85.7	507	35.3	214.3	507
Dawen, Guizhou	120	3.4	35.3	160	0.7	228.6	548	88.2	571.4	548
Lung Cam, Veitnam	2.6	0.06	42.9	2.4	0.03	96	124	107.3	240	124
Spiti, India	1	3.4	0.3	1	0.7	1.4	386	0.7	3.6	386
Guryul Ravine, India	20	3.4	5.9	8	0.7	11.4	94	14.7	28.6	94
Zal, Iran	40	3.4	11.8	120	0.7	171.4	1357	29.4	428.6	1357
Uomo, Italy	120	3.4	35.3	90	0.7	128.6	264	88.2	321.4	264
Spitsbergen	40	3.4	11.8	60	0.7	85.7	629	29.4	214.3	629
West Blind Fiord, Arctic	20	3.4	5.9	100	0.7	142.9	2329	14.7	357.1	2329
Ursala Creek, Alberta	1	0.5	2	100	0.7	142.9	7043	5	357.1	7043
Sawtooth Range, Arctic				240	0.9	267	4520	5	667.5	4541

LSR and BAR for Changhsingian (uppermost Permian) and Griesbachian (lowermost Triassic) units from select localities. Study area is added as Sawtooth Range, but the duration of the Cape Butler Member is from the Griesbachian to Dienerian, with data from West Blind Fiord used to calculate LSR and BAR. See Section 3.6 for details on calculations; data from Algeo and Twitchett (2010) GSA data repository 2010283.